2016-06

Thermal creep force: analysis and application

Wolfe, David M.

Monterey, California: Naval Postgraduate School

NAVAL POSTGRADUATE SCHOOL

MONTEREY, CALIFORNIA

DISSERTATION

THERMAL CREEP FORCE: ANALYSIS AND APPLICATION

by

David M. Wolfe

June 2016

Dissertation Supervisor: Andres Larraza

Approved for public release; distribution is unlimited

THIS PAGE INTENTIONALLY LEFT BLANK

REPORT DOCUMENTATION PAGE			*Form Approved OMB No. 0704–0188*
Public reporting burden for this collection of information is estimated to average 1 hour per response, including the time for reviewing instruction, searching existing data sources, gathering and maintaining the data needed, and completing and reviewing the collection of information. Send comments regarding this burden estimate or any other aspect of this collection of information, including suggestions for reducing this burden, to Washington headquarters Services, Directorate for Information Operations and Reports, 1215 Jefferson Davis Highway, Suite 1204, Arlington, VA 22202-4302, and to the Office of Management and Budget, Paperwork Reduction Project (0704-0188) Washington, DC 20503.			
1. AGENCY USE ONLY ***(Leave blank)***	**2. REPORT DATE** June 2016	**3. REPORT TYPE AND DATES COVERED** Doctoral Dissertation	
4. TITLE AND SUBTITLE THERMAL CREEP FORCE: ANALYSIS AND APPLICATION			**5. FUNDING NUMBERS**
6. AUTHOR(S) David M. Wolfe			
7. PERFORMING ORGANIZATION NAME(S) AND ADDRESS(ES) Naval Postgraduate School Monterey, CA 93943-5000			**8. PERFORMING ORGANIZATION REPORT NUMBER**
9. SPONSORING /MONITORING AGENCY NAME(S) AND ADDRESS(ES) N/A			**10. SPONSORING / MONITORING AGENCY REPORT NUMBER**
11. SUPPLEMENTARY NOTES The views expressed in this thesis are those of the author and do not reflect the official policy or position of the Department of Defense or the U.S. Government. IRB Protocol number ____N/A____.			
12a. DISTRIBUTION / AVAILABILITY STATEMENT Approved for public release; distribution is unlimited			**12b. DISTRIBUTION CODE**

13. ABSTRACT (maximum 200 words)

The existence of two motive forces on a Crookes radiometer has complicated the investigation of either force independently. The thermal creep shear force, in particular, has been subject to differing interpretations of the direction in which it acts and its order of magnitude. A horizontal vane radiometer design is provided, which isolates the thermal creep shear force. The horizontal vane radiometer is explored through experiment, kinetic theory, and the Direct Simulation Monte Carlo (DSMC) method. The qualitative agreement between the three methods of investigation is good. The quantitative agreement between the three methods of investigation is better than an order of magnitude in the cases examined. The thermal creep force is found to act from the hot side to the cold side of the vane. The peak in the radiometer's angular speed as a function of pressure is found to be explained as much by the behavior of the drag force as by the behavior of the thermal creep force. In addition, this dissertation provides scaling laws between millimeter-scale and micron-scale horizontal vane radiometers, a design of a microelectromechanical system (MEMS) horizontal vane radiometer, and conceptual designs of two MEMS energy harvesting devices that exploit the thermal creep force.

14. SUBJECT TERMS rarefied gas flows, kinetic theory, numerical methods			**15. NUMBER OF PAGES** 77
			16. PRICE CODE
17. SECURITY CLASSIFICATION OF REPORT Unclassified	**18. SECURITY CLASSIFICATION OF THIS PAGE** Unclassified	**19. SECURITY CLASSIFICATION OF ABSTRACT** Unclassified	**20. LIMITATION OF ABSTRACT** UU

NSN 7540–01-280-5500 Standard Form 298 (Rev. 2–89)
Prescribed by ANSI Std. 239–18

THIS PAGE INTENTIONALLY LEFT BLANK

Approved for public release; distribution is unlimited

THERMAL CREEP FORCE: ANALYSIS AND APPLICATION

David M. Wolfe
Commander, United States Navy
B.S., United States Naval Academy, 2000
M.S., Naval Postgraduate School, 2006

Submitted in partial fulfillment of the
requirements for the degree of

DOCTOR OF PHILOSOPHY IN APPLIED PHYSICS

from the

NAVAL POSTGRADUATE SCHOOL
June 2016

Approved by: Dr. Andres Larraza
Associate Professor of Physics
Dissertation Supervisor

Dr. Joseph Hooper
Assistant Professor of Physics

Dr. Dragoslav Grbovic
Assistant Professor of Physics

Dr. Garth Hobson
Professor of Mechanical and
Aerospace Engineering

Dr. Alejandro Garcia
Professor of Physics and Astronomy

Approved by: Dr. Kevin Smith, Chair, Department of Physics

Approved by: Douglas Moses, Vice Provost for Academic Affairs

THIS PAGE INTENTIONALLY LEFT BLANK

ABSTRACT

The existence of two motive forces on a Crookes radiometer has complicated the investigation of either force independently. The thermal creep shear force, in particular, has been subject to differing interpretations of the direction in which it acts and its order of magnitude. A horizontal vane radiometer design is provided, which isolates the thermal creep shear force. The horizontal vane radiometer is explored through experiment, kinetic theory, and the Direct Simulation Monte Carlo (DSMC) method. The qualitative agreement between the three methods of investigation is good. The quantitative agreement between the three methods of investigation is better than an order of magnitude in the cases examined. The thermal creep force is found to act from the hot side to the cold side of the vane. The peak in the radiometer's angular speed as a function of pressure is found to be explained as much by the behavior of the drag force as by the behavior of the thermal creep force. In addition, this dissertation provides scaling laws between millimeter-scale and micron-scale horizontal vane radiometers, a design of a microelectromechanical system (MEMS) horizontal vane radiometer, and conceptual designs of two MEMS energy harvesting devices that exploit the thermal creep force.

THIS PAGE INTENTIONALLY LEFT BLANK

TABLE OF CONTENTS

THIS PAGE INTENTIONALLY LEFT BLANK

LIST OF FIGURES

THIS PAGE INTENTIONALLY LEFT BLANK

ACKNOWLEDGMENTS

I would like to thank my dissertation advisor and committee for all their help with this project. Specifically, I would like to thank Andres Larraza for conceptualizing the horizontal vane radiometer and overseeing the experiments, Alejandro Garcia for providing guidance as I learned the DSMC method, Dragoslav Grbovic for insight into MEMS technology, and Joseph Hooper for introducing me to the Department of Defense High Performance Computing Modernization Program. Additionally, I would like to thank my parents for proofreading and providing valuable suggestions to improve the text of this dissertation. Finally, I would like to thank my wife and children, who I love dearly.

THIS PAGE INTENTIONALLY LEFT BLANK

I. INTRODUCTION

The purpose of this dissertation is twofold: first, to confirm and improve upon the existing understanding of the thermal creep force, and second, to design Microelectromechanical System (MEMS) energy harvesting devices that utilize the thermal creep force. Recent research using numerical methods that shows the force acting in a direction opposite to that originally found by Osbourne Reynolds motivates the need to confirm the existing understanding of the thermal creep force [1], [2]. The fact the solution to the Boltzmann equation with the Chapman-Enskog correction for thermal creep force has been reported to significantly over-predict experimental results and has not been fully accepted by the community motivates the need to improve on the existing understanding of the thermal creep force [3].

This chapter provides a historic overview of the Crookes radiometer, which led to the discovery of the thermal creep force. Chapter II presents the results of an experiment on a novel horizontal vane radiometer designed to isolate the thermal creep force from the other motive force on the Crookes radiometer. These results confirm Reynolds's report of the direction in which the thermal creep force acts. Chapter III considers several edge and kinetic theory corrections to the thermal creep force result given by Scandurra *et al*. [4]. These corrections allow the result, when combined with the drag force, to provide a reasonable prediction of the angular speeds reported in Chapter II. In Chapter IV, the results of numerical simulations of the experiment in Chapter II are presented. The purpose of the simulations is to provide direct values of the thermal creep and drag forces. These results lend credence to the adjustments made in Chapter III. In Chapter V, a comparison of experimental, theoretical, and simulation results is given. Finally, Chapter VI provides a scaling law for the thermal creep force on MEMS vanes and two designs of energy harvesting devices.

A. THERMAL CREEP

Thermal transpiration, or thermal creep, is the flow of a gas over a surface due to a temperature gradient in the gas parallel to the surface. The force on the gas is equal and

opposite to the force on the surface. The force exerted on a surface by a gas with a temperature gradient is thus called the thermal creep force. The force is most famously demonstrated by the Crookes radiometer (see Figure 1).

Figure 1. A Crookes Radiometer

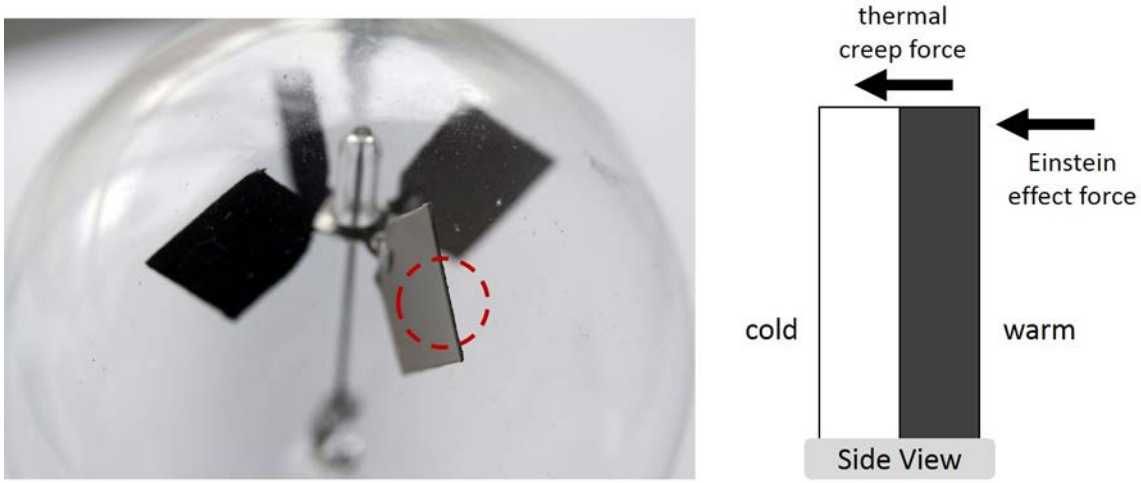

The figure on the right is an edge view of the vane and not to scale. In commercial Crookes radiometers, typical vanes are 1.5 cm x 1.5 cm and thickness is usually on the order of 0.1 mm. The thermal creep force acts on the edge parallel to the temperature gradient. The Einstein effect acts on the surfaces perpendicular to the temperature gradient.

William Crookes published the atomic weight of Thallium in 1873. He weighed Thallium salts at atmospheric pressure and reduced pressure to quantify the buoyant force on his sample and determine what the weight would be in a perfect vacuum. He found that the weight measured at reduced pressures was sensitive to the light source he used to illuminate the scale. At the time it was believed that a hot object would weigh less than a cold object of similar mass because of upward air flow near the hot object or condensation on the cold object [5]. Crookes recognized these effects should decrease with decreasing pressure, but the effect he was observing did not. He designed the Crookes radiometer and other experiments to study the effect. In 1874 he ascribed the observed motion to repulsion by radiant heat which he theorized is present at all pressures but masked by air currents at higher pressures [6]. This is not the correct explanation of

the motion. Though radiation pressure does exist, it produces a small force and would tend to move the vanes with the black side leading contrary to the observed motion.

The same year Crookes published his results and analysis, Osbourne Reynolds published an analysis ascribing the effects to the transfer of momentum between the surface and gas molecules during evaporation, condensation, and heat transfer [7]. Osbourne Reynolds further explains that an evaporating molecule leaves the surface with a certain momentum and the surface gains an equal and opposite momentum. A molecule undergoing condensation arrives with a certain momentum which is transferred to the surface. A molecule that transfers heat with a surface during a collision departs with a different momentum than with which it arrived the balance of which is conserved by transfer to or from the surface.

Reynolds continued to study the transfer of momentum between a surface and gas during heat transfer by experimenting with a porous plate with its two sides held at different temperatures [8]. He was able to conduct his experiments at atmospheric pressure because the ratio of a characteristic length of the pores to the mean free path of air at atmospheric pressure is similar to the ratio of the characteristic length of a vane in a Crookes radiometer to the mean free path of air at the pressures where motion can be observed. He found that gas would flow through the pores from the cold side of the plate to the hot side of the plate and named this flow “thermal transpiration” in 1879. Molecules entering the pores from the cold side of the plate tend to gain heat and therefore velocity as they travel through the pore while molecules entering the pores from the hot side of the plate tend to lose heat and therefore velocity as they travel through the pore. These effects combine for a net velocity and flow from the cold side to the hot side. This same flow occurs over the edge of the vanes in a Crookes radiometer creating a thermal creep force on the vane directed from the hot side to the cold side.

B. THE ENERGY ACCOMMODATION COEFFICIENT

Also in 1879, but after reading Reynolds’ paper, James Maxwell further refined the theory of thermal creep by considering the details of the collisions between gas molecules and the surface [9]. Maxwell considered two types of collisions. Reflected

gases behave as if the surface was perfectly smooth and elastic. No energy is transferred between a reflected gas and the surface, and the tangential components of the molecules' velocities are unchanged by the collision. Reflected gas does not contribute to thermal creep. Absorbed-and-evaporated gases behave as if they were "entangled in the stratum of spheres" that Maxwell imagined coving the surface. Energy is transferred between an absorbed-and-evaporated gas and the surface. Absorbed-and-evaporated gas molecules leave the surface in a random direction with a speed equivalent to the surface temperature. Absorbed-and-evaporated gas is responsible for thermal creep. The magnitude of the thermal creep effect is thus related to the ratio of the number of gas molecules that are absorbed-and-evaporated to the total number of gas-surface collisions in a sample.

Today, the extent to which energy is transferred in a collision between a gas molecule and a surface is expressed as the accommodation coefficient α. An accommodation coefficient of zero is equivalent to a perfectly reflected gas. An accommodation coefficient of one is equivalent to a perfectly absorbed-and-evaporated gas. Other models use separate accommodation coefficients for energy, normal momentum, and tangential momentum calculations; but the Maxwell model implies those values are the same. The accommodation coefficients of real gases and surfaces are a function of the colliding molecules and the temperature. The modified Boule formula estimates the accommodation for clean surfaces below 500 K, where μ is the ratio of the molecular weight of the gas to the molecular weight of the surface.

$$\alpha = \frac{2.4\mu}{(1+\mu)^2} \tag{1.1}$$

Surfaces absorb layers of molecules when exposed to air [10]. A gas molecule colliding with a "dirty" surface will thus collide with a molecule of a similar molecular weight (μ equals one) regardless of the material composition of the underlying surface. From equation (1.1), the accommodation coefficient equals its maximum value of 0.6 when μ equals one. Thus, 0.6 is a reasonable estimate for the energy accommodation coefficient of a "dirty" surface in air. Nevertheless, it should be noted accommodation values greater

than the maximum value of the modified Boule formula have been observed and are commonly assumed in other studies.

C. THE EINSTEIN EFFECT

Thermal creep is a shear force acting on the edges of the vanes in a Crookes radiometer. In 1924, Albert Einstein identified a normal force acting on the perimeter of the vertical faces as well [11]. He imagined a chamber of rarified gas with a temperature gradient and no net mass flow. A flat surface smaller than a mean free path of the gas placed in the chamber normal to the temperature gradient would experience a force toward the cold side as the same number of molecules per unit time would collide with it from the cold side as from the hot side because of the no net mass flow requirement while the particles coming from the hot side would have a higher velocity. A flat surface larger than a mean free path of the gas in the same chamber oriented in the same way would not have a net force on its center once the pressure had time to equalize and reestablished the no mass flow requirement. There would nevertheless be a transition region between the center of the surface where no net force is experienced and the region beyond the surface where a small surface placed in the chamber would experience a force. This transition occurs over a mean free path wide perimeter of the surface. The vanes of the Crookes radiometer have a net normal force in this perimeter directed from the hot side to the cold side. A mathematical development of the Einstein effect is included in Appendix A.

Thermal creep and the Einstein effect provide the theoretical bases for the two motive forces on the Crookes radiometer. Subsequent work on the topic has focused on mathematical refinement of the theories and novel radiometer designs [3]. One alternative design is the Hettner radiometer (see Figure 2). In 1924, M. Czerny and G. Hettner designed an experiment to measure the shear pressure or force on a plate with a uniform temperature from the thermal creep caused by a parallel plate with a temperature gradient [12]. This design does not experience the Einstein effect because the plate face is parallel to the temperature gradient.

Figure 2. Hettner Radiometer

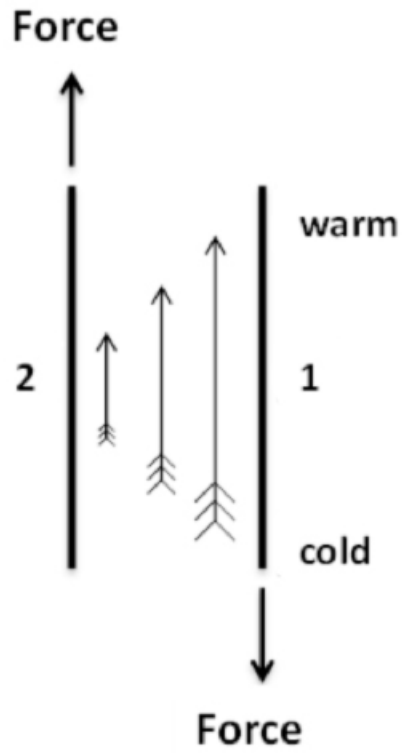

Plate 1 has a temperature gradient and plate 2 has a uniform temperature. The temperature gradient establishes thermal creep (arrows with fletchings). Plate 1 experiences thermal creep force while plate 2 experiences drag from the thermal creep.

II. A HORIZONTAL VANE RADIOMETER EXPERIMENT

We designed a horizontal vane radiometer (see Figure 3) that, like the Hettner radiometer, has the temperature gradient parallel to the vane face but, like the Crookes radiometer, is free to rotate around a spindle [13].

Figure 3. The Crookes and Horizontal Vane Radiometers

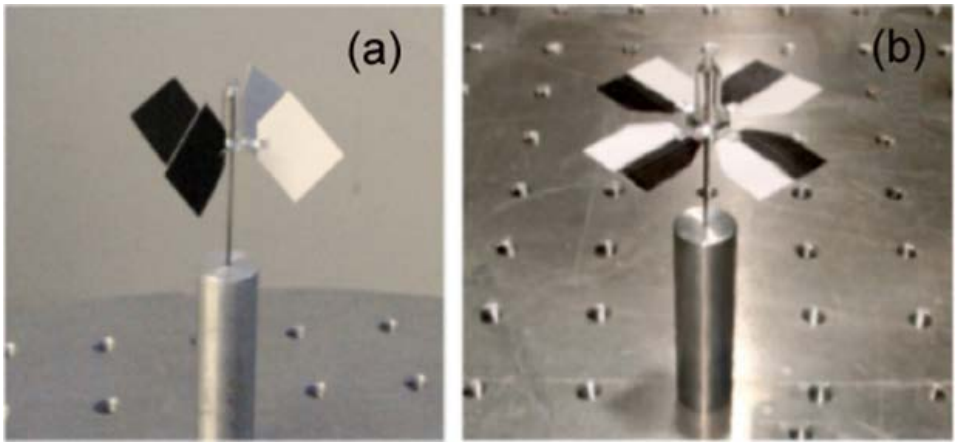

(a) The Crookes radiometer experiences thermal creep forces and the Einstein effect. (b) The horizontal vane radiometer experiences thermal creep forces but no Einstein effect.

The angular speeds of horizontal vane radiometers were observed over a range of pressures with mean free paths from 5 mm to 0.2 mm. Two types of horizontal vane radiometers were constructed. The narrow vane radiometer had 8 mm by 16 mm vanes. The wide vane radiometer had 16 mm by 16 mm vanes. The vanes were constructed from high gloss photo paper. Half of the non-glossy side was printed with black LaserJet ink. Two pieces of paper cut into the shape of the vanes were glued together glossy side to glossy side so that both the upper and lower horizontal surfaces would have a white side and a black side. The vanes on both radiometers were connected to the spindle with 4 mm stems.

A high intensity radiant heat projector was used to illuminate the radiometers. The temperature profile that developed on the vanes when illuminated was observed with a FLIR SC8200 camera outside of the vacuum chamber and a FLIR ThermoVision A20

camera inside of the vacuum chamber. The temperature profile was not observed to be sensitive to pressure. Under illumination, the vanes developed a 9 K temperature difference between the black and the white side with the transition in temperature mostly occurring in a sharp gradient in the center of the vane with a characteristic length of 3.5 mm. The radiometers were tested in a 18-inch diameter 12-inch-high Pyrex bell jar on a highly reflective test stand so that both the upper and lower horizontal surfaces would be illuminated. Figure 4 reports the results of these experiments at the pressures tested. [14] shows video of horizontal vane radiometers rotating at 10 mTorr.

Figure 4. Angular Speed (Experiment)

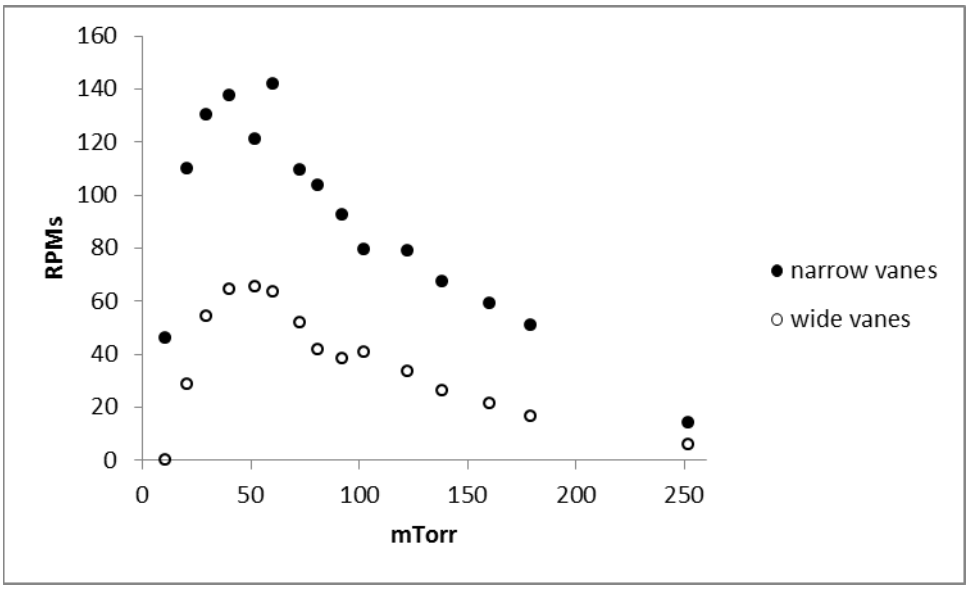

The narrow vanes are 8 mm by 16 mm and the wide vanes are 16 mm by 16 mm. Both radiometers have four vanes. Vanes of both radiometers have a 4 mm stem connecting them to the spindle axis. The temperature difference on the vanes is 9 K. The characteristic length of the temperature gradient is 3.5 mm. The observed motion is with the white (cold) side leading. Angular speed is reported in revolutions per minute (RPMs).

III. THE HORIZONTAL VANE RADIOMETER THEORY

The theory of thermal creep explains why the horizontal vane radiometer rotates, but an understanding of why the angular speed peaks and is a function of the vanes' widths requires careful examination of the details of both the drag force and thermal creep shear force on the vanes. We follow the development of Wolfe *et al*. [15].

A. THERMAL CREEP

For an angular speed of 10 radians per second, the furthest edges of the vanes will move a distance between 2 μm and 80 nm during a mean free time between collisions for the pressures in our experiment. Because these distances are small relative to the widths of the vanes in our experiment, a temperature gradient in the gas over the vane created by collisions between the gas and the vane will remain over the vane despite the vane's rotation justifying a quasi-static assumption for the calculation of the thermal creep force on a moving radiometer with the observed velocities.

Molecules in a gas with a temperature gradient have a Chapman-Enskog distribution of velocities [16]. The probability density function f is the sum of the Maxwell-Boltzmann distribution function f_0 and the Chapman-Enskog correction f_1.

$$f = f_0 + f_1 \tag{3.1}$$

The Chapman-Enskog correction f_1 for a gas with a temperature gradient is

$$f_1 = A v_y \left(\frac{5}{2} - \beta \left(v_x^2 + v_y^2 + v_z^2 \right) \right) f_0 \tag{3.2}$$

$$f_0 = \left(\frac{\beta}{\pi} \right)^{\frac{3}{2}} e^{-\beta \left(v_x^2 + v_y^2 + v_z^2 \right)} \tag{3.3}$$

$$\beta = \frac{m}{2 k_B T} \tag{3.4}$$

$$A = \frac{15}{32 n \sigma_{CS} T} \sqrt{\frac{\pi m}{k_B T}} \frac{dT}{dy} \tag{3.5}$$

where v is the velocity, m is the mass, n is the number density, $\sigma_{CS} = \pi d^2$ is the hard-sphere collision cross section of the molecules with diameter d, k_B is Boltzmann's constant, T is the gas temperature, and dT/dy is the temperature gradient in the gas [16].

The net thermal creep pressure Δp_{TC} on a surface in the y-z plane with the gas in the positive x direction is determined by integrating the longitudinal momentum transfer of the gas along the surface of the plate with accommodation coefficient α [4].

$$\Delta p_{TC} = nm \int_{-\infty}^{0} dv_x \int_{-\infty}^{\infty} dv_z \int_{-\infty}^{\infty} dv_y v_y v_x f\left(\vec{v}\right) \alpha \tag{3.6}$$

The Maxwellian term integrates to zero but the Chapman-Enskog term survives providing the following result.

$$\Delta p_{TC} = \frac{15}{64\sqrt{2}} \frac{k_B}{\sigma_{CS}} \frac{dT}{dy} \alpha \tag{3.7}$$

The thermal creep force F_{TC} is this pressure multiplied by the area over which it acts A_{TC}. If L_{TC} is the length of a rectangle perpendicular to the temperature gradient and W_{TC} is the width along the temperature gradient, we have

$$F_{TC} = \Delta p_{TC} A_{TC} = \Delta p_{TC} L_{TC} W_{TC}. \tag{3.8}$$

Assuming the temperature gradient in the gas is roughly constant in the area where the thermal creep force acts, the temperature gradient term can be replaced by

$$\frac{dT}{dy} \approx \frac{\Delta T}{W_{Ggas}}, \tag{3.9}$$

where ΔT is the temperature difference between the hot and the cold sides of the surface and W_{Ggas} is the width of the temperature gradient in the gas.

The width of the temperature gradient established in a low-pressure gas by a surface with a temperature gradient is wider than the temperature gradient on the surface W_{Gsurf} by a length equal to the slip length [17], or

$$W_{Ggas} = W_{Gsurf} + 2\lambda \frac{2-\alpha}{\alpha} \tag{3.10}$$

where λ is the mean free path of the gas and α is the accommodation coefficient. The mean free path is related to the particle number density n and collision cross section as $\lambda = 1/\sqrt{2}n\sigma_{CS}$.

The physical meaning of equation (3.10) can be understood by considering the two extreme values of α. When the accommodation equals zero, the width of the gradient in the gas is infinite. There is thus no gradient when there is no energy transfer between the surface and the gas. When the accommodation equals one, the width of the gradient in the gas is the width of the gradient on the surface plus two mean free paths. The gradient thus extends one mean free path further on each side in the gas than in the surface.

In the horizontal vane radiometer experiment, there are four temperature gradients in the plane of each vane (see Figure 5).

Figure 5. Temperature Gradients on a Horizontal Vane

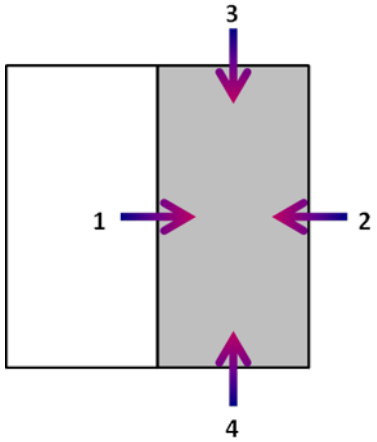

The white (cold) side of the vane is assumed to have a temperature similar to ambient temperature and the grey (hot) side is warmer than ambient temperature.

Temperature gradient #1 causes the force F_{TC1} which causes the rotation of the radiometer and is a convenient starting point for the calculation of the total thermal creep force on the vane. We will treat the effects of the other temperature gradients as apparent modifications of the force from temperature gradient #1.

Temperature gradient #2 creates a force which opposes the rotation. The magnitude of this force is less than the magnitude of the force created by temperature gradient #1 because the portion of temperature gradient #2 which is not over the vane does not create a force, i.e.

$$F_{TC} = xF_{TC1}, \tag{3.11}$$

where x is a numerical factor between zero and one representing the fraction of the force from temperature gradient #1 which is offset by the force from temperature gradient #2.

The net force created by temperature gradients #3 and #4 is zero, but these gradients decrease the magnitude of temperature gradient #1 near the edges. This has the effect of decreasing the apparent length over which the net thermal creep pressure from temperature gradient #1 acts. The length correction is the slip length times the numerical factor β or

$$L_{TC}' = L_{TC1} - \beta\lambda\frac{2-\alpha}{\alpha}. \tag{3.12}$$

The width over which temperature gradient #1 acts is the smaller of either the width of the vane W_V or the width of the temperature gradient in the gas. Putting this together with equations (3.7) to (3.12) gives the following expression for the net thermal creep force on the two sides of a single vane in the horizontal vane radiometer experiment:

$$F_{TC} = \frac{15x}{32\sqrt{2}}\frac{k_B}{\sigma_{CS}}\Delta T\alpha L'\min\left(\frac{W_V}{W_{Ggas}},1\right), \tag{3.13}$$

where L' is the length of the vane with the slip length correction.

Figure 6 shows the net thermal creep force predicted by this equation for the vanes in the horizontal vane radiometer experiment assuming numerical factors of $x = 0.5$ and $\beta = 0.5$ for equations (3.11) and (3.12). These values follow from the

assumption that the gas temperature at the edge is equal to the average of the temperature of the hot side of the vane and the ambient temperature. We assumed an accommodation coefficient of $\alpha = 0.6$. An even higher value of the accommodation would result in the force rising more quickly as a function of pressure and asymptotically approaching a higher value. The pressure dependence of the force is a result of the slip length corrections in the width of the gradient in the gas and the apparent length of the vane.

Figure 6. Thermal Creep Force (Theory)

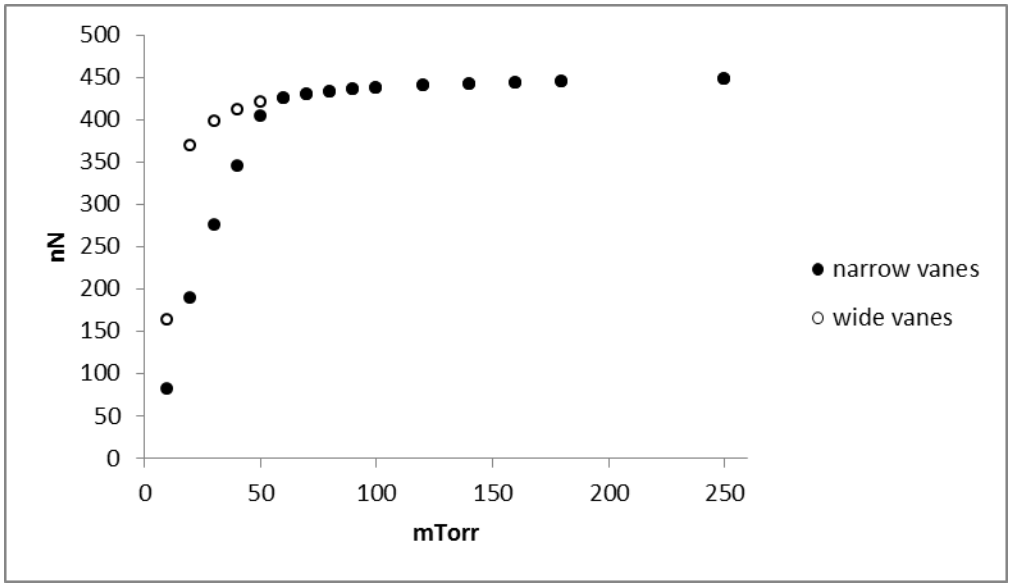

The narrow vanes are 8 mm by 16 mm and the wide vanes are 16 mm by 16 mm. The temperature difference on both vanes is 9 K. The characteristic length of the temperature gradient on the surface is 3.5 mm. The accommodation coefficient is 0.6. At 60 mTorr and greater pressure the forces are similar on the narrow and wide vanes. A positive force is directed from the hot side to the cold side.

B. DRAG FORCE

The dominant drag force on a thin plate oriented parallel to the flow is skin friction. The skin friction on an object is a function of the fluid density ρ, velocity U, drag coefficient C_D, and the surface area A.

$$F_D = \frac{1}{2}\rho U^2 C_D A \tag{3.14}$$

The drag coefficient is a function of the Reynolds number. The Reynolds number is a function of the fluid density, velocity, the length over which the flow varies (the width of the vane in this case) W, and the dynamic viscosity of the fluid (μ).

$$\mathrm{Re} = \frac{\rho U W}{\mu} \tag{3.15}$$

Stokes' drag occurs at very low Reynolds numbers (*Re < 1*). The Reynolds numbers for every trial in the horizontal vane radiometer experiment was less than 0.02. Therefore, all the trials in this experiment were securely in the Stokes' drag regime. The drag coefficient for Stokes' drag is proportional to the inverse of the Reynolds number where δ is a numerical factor.

$$C_D = \frac{\delta \mu}{\rho U W} \tag{3.16}$$

For thin plates oriented parallel to the flow, a theoretical value of 4.12 for δ has been calculated [18]. On the other hand, an experimental value of 5.91 has been observed [19]. Thus, for uniform flow past a flat plate the Stokes drag force on both sides of the plate is

$$F_D = 2\frac{1}{2}\rho U^2 C_D L W = 5.91 U \mu L, \tag{3.17}$$

where *L* is the dimension perpendicular to the flow (the length of the vane in this case).

The Stokes' drag equation does not take edge effects into account. Each edge parallel to the flow that is immersed in the fluid adds the empirically determined correction to the drag force equation [20]

$$F_{edge} = 1.6 U \mu W. \tag{3.18}$$

At low pressure there is an apparent decrease in the dynamic viscosity due to the slip length [17]

$$\mu' = \frac{\mu W}{W + 2\lambda \dfrac{2-\alpha}{\alpha}}. \tag{3.19}$$

Chapman's expression for the dynamic viscosity [16],

$$\mu = \frac{5\pi}{32}\rho C \lambda, \tag{3.20}$$

which accounts for variable collision rate, improves on Maxwell's classical estimate, $\mu = \rho C\lambda/3$. Here C is the mean speed of a gas molecule. Note that μ is pressure independent. The substitutions $\rho=nm$ and $C = \sqrt{8k_BT/\pi m}$, where m is the molecular mass, express μ' in terms of kinetic theory quantities

$$\mu' = \frac{5\sqrt{\pi}}{16} \frac{\sqrt{mk_BT}W}{\sigma_{CS}W + \frac{\sqrt{2}}{n}\frac{2-\alpha}{\alpha}}. \tag{3.21}$$

It is not obvious that the slip length correction should apply to the drag on the edges but a correction is necessary for the edge correction to the drag force to be equal to zero at zero pressure. We will assume the correction takes a similar form for both the skin friction and the edge drag.

For a uniformly rotating vane, including edge effects, the drag force is

$$F_D = \omega\left(L_S + \frac{L}{2}\right)\mu'\left(5.91L + 3.2W\right), \tag{3.22}$$

where L_s is the length of the stem. Figure 7 shows the drag force predicted by this equation for the vanes in the horizontal vane radiometer experiment at 10 rad/s.

Figure 7. Drag Force at 10 rad/s (Theory)

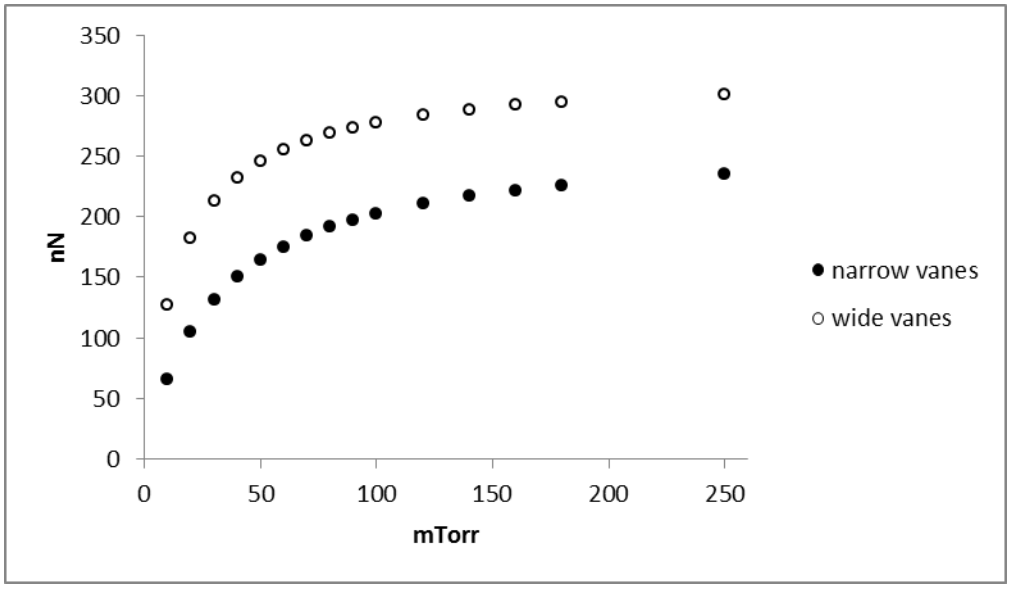

The narrow vanes are 8 mm by 16 mm and the wide vanes are 16 mm by 16 mm. Both vanes have a 4 mm stem connecting them to the spindle axis. The accommodation coefficient is 0.6.

C. ANGULAR SPEED

Assuming negligible mechanical friction in the spindle, the equilibrium angular speed ω of the horizontal vane radiometer occurs when the drag torque equals the thermal creep torque. Because the drag force is linearly related to the angular speed, we can define the drag force per unit angular velocity f_D as

$$f_D = \frac{F_D}{\omega}. \tag{3.23}$$

Thus, in terms of thermal creep,

$$\omega = \frac{r_{tc} F_{TC}}{r_d f_D}. \tag{3.24}$$

where r_{tc} and r_d are the effective moment arms of the thermal creep and drag forces respectively. Please note that in our experiment's geometry, the drag force moment arm is 121% and 125% of the thermal creep force moment arm for the narrow and wide vane respectively because the thermal creep force acts uniformly along the length of the vane while the drag force increases further from the rotation axis. Since both forces will scale linearly with the number of vanes it is possible to examine the torques on a single vane to predict the angular speed of a radiometer with four vanes. Figure 8 shows the predicted angular velocity that results by using the expressions (3.13) and (3.22) in the above equation.

Figure 8. Angular Speed (theory)

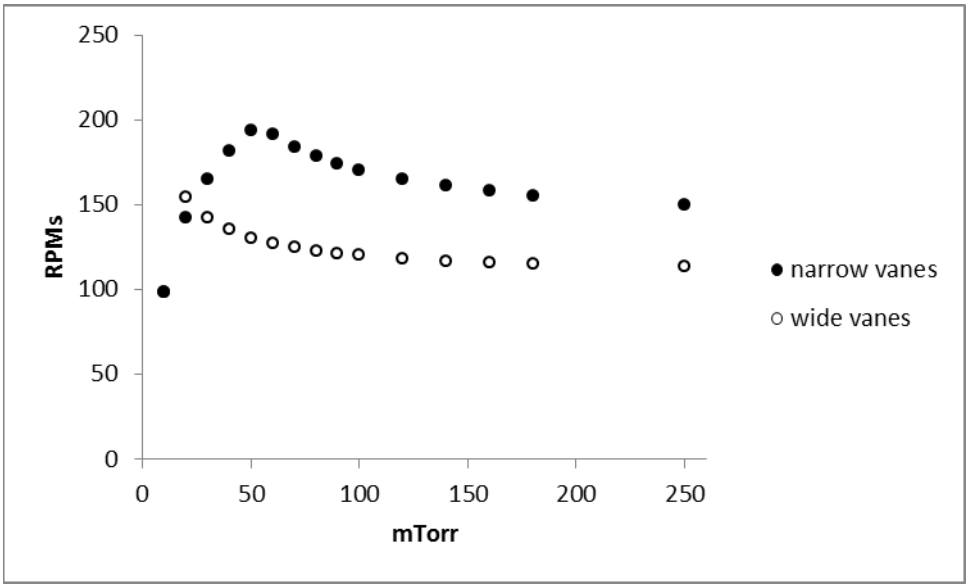

The narrow vanes are 8 mm by 16 mm and the wide vanes are 16 mm by 16 mm. Both vanes have a 4 mm stem connecting them to the spindle axis. The temperature difference on both vanes is 9 K. The characteristic length of the temperature gradient on the surface is 3.5 mm. The accommodation coefficient is 0.6. Positive angular speed represents rotation with the cold side leading. The angular speeds are similar at 10 mTorr.

THIS PAGE INTENTIONALLY LEFT BLANK

IV. HORIZONTAL VANE RADIOMETER SIMULATIONS

Direct Simulation Monte Carlo (DSMC) is a method of determining continuum properties of a fluid by simulating individual particles of the fluid [21]. Simulation particles are weighted to represent multiple fluid particles to reduce computational effort. The Navier-Stokes equations of continuum gas dynamics are a computationally easier method of determining the same quantities but provide inaccurate results when the mean free path of the gas approaches a representative length scale of the system. For this reason the DSMC method is most usefully applied to rarefied gases where the mean free path of the gas is of the same order or larger than a characteristic length of the system.

DSMC programs divide the simulation space into grid cells. Particles are initially created in random locations with a Gaussian velocity distribution centered on an assigned fluid velocity. At each time step, particles move a distance equal to their velocity times the time step. The behavior of particles that reach the boundary of the simulation space is determined by the boundary conditions of the simulation. Particles that impact a surface in the simulation space undergo either specular or diffuse reflection depending on the simulation inputs. Momentum transfer between the surface and colliding particles is recorded for subsequent calculation of the pressure on the surface with the mass of a particle equaling the mass of a molecule times the number of molecules represented by a particle in the simulation.

After the particles have completed their motion, particles are randomly selected for collision. The probability that an individual particle will be selected for collision is determined by the mean free time between collisions of molecules in the gas being simulated divided by the time step. Collision partners are then chosen from within the same grid cell. The collision partners are assigned new velocities that conserve energy and momentum.

Statistical fluctuations in DSMC results can be averaged out by decreasing the number of molecules represented per simulation particle, increasing the amount of time simulated, or averaging the results of multiple trials. Systemic errors can be introduced

by large grid sizes or time steps. The truncation error introduced by the grid size is proportional to the ratio squared of the length of a side of the grid cell to the mean free path of the gas [22]. The truncation error introduced by the time step is proportional to the ratio squared of the time step to the mean free time between collisions of molecules in the gas [23].

SPARTA (Stochastic PArallel Rarefied-gas Time-accurate Analyzer) is an open-source DSMC program developed at Sandia National Laboratories [24]. We used it in this research to determine separately the shear pressures caused by drag and thermal creep on vanes similar to those in the horizontal vane radiometer experiment at the range of pressures tested in the experiment. We used the February 21, 2015 version of SPARTA with one modification. The modification was the removal of the command to terminate the trial if a particle collides with an interior surface of the vane. This feature was in the code to ensure objects in the simulation space are airtight, but occasionally the algorithm used by SPARTA to distinguish between interior and exterior collisions mistakenly classifies a collision in our geometry. We checked the simulated vanes for airtightness before running the trials on the modified program. We ran the trials on the Hamming supercomputer at the Naval Postgraduate School and the Spirit supercomputer at the Air Force Research Laboratory. Each trial took five thousand to 50 thousand CPU hours to complete.

A. THERMAL CREEP SIMULATIONS

We ran a total of 30 thermal creep simulations encompassing both the narrow vane and the wide vane at the 15 pressures tested in the experiment. In each trial, we simulated a single stationary vane and the shear pressure on the vane was the output. We divided each trial into 10 time segments which reported 10 separate average shear pressures. This confirmed the behavior was not transitory and allowed us to calculate a standard deviation between the 10 segments to quantify the uncertainty in the output.

In SPARTA, geometry objects have a single assigned temperature and cannot touch other objects. To simulate a vane with a temperature gradient, we created nine

objects in the simulation space. Figure 9 is an overhead view of the wide and narrow vane as modeled in SPARTA.

Figure 9. Vanes as Modeled in SPARTA

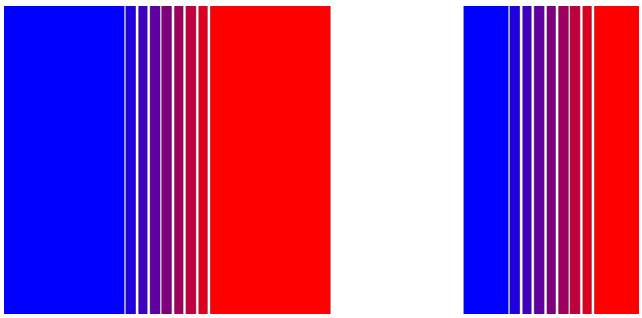

The wide and narrow vanes are each divided into nine segments separated by two Angstroms. Each segment has a single assigned temperature.

The cold side of the vanes was assigned a temperature of 293 K. The hot side of the vanes was assigned a temperature of 302 K. Each intermediate segment was 1.125 K warmer than its colder neighbor. All nine rectangular boxes which comprised a vane were 16 mm long and 0.1 mm thick. The seven boxes in the gradient region were 0.5 mm wide which from equation (3.10) is thin enough to create a smooth gradient in the gas at all pressures simulated. The two end boxes were 6.25 mm wide for the wide vane and 2.25 mm wide for the narrow vane.

The simulation space was 18 mm by 26 mm by 10 mm for the narrow vane simulations and 26 mm by 26 mm by 10 mm for the wide vane simulations. This ensured at least one mean free path between the vane and the boundary at all pressures simulated. The boundary condition was inflow and outflow so particles whose trajectory took them outside the simulation space would no longer be simulated and new particles would be created and entered into the simulation space throughout the trial. The size of the grid cells was varied with pressure so that each edge of a grid cell equaled half of a mean free path in length. The total number of grid cells ranged from 280 for the narrow vane at 10 mTorr to over 6 million for the wide vane at 250 mTorr.

Particles were created with an initial average temperature of 293 K. Eight-hundred and fifty million particles were initially created in the narrow vane simulations

and 1.2 billion particles were initially created in the wide vane simulations. This ensured there was an average of 200 particles per grid cell at the highest pressure trials. The lower pressure trails had more than 200 particles per grid cell since the grid cells were larger and fewer in the lower pressure trials. The number of molecules represented by a single simulation particle varied with pressure. This value varied from 1.8 million molecules per simulation particle at 10 mTorr to 45 million molecules per simulation particle at 250 mTorr. 79% of the particles were diatomic Nitrogen and 21% of the particles were diatomic Oxygen. We used the variable soft sphere collision model.

The time step was 100 ns. This value is one fourth the mean free time between collisions at 250 mTorr and a smaller fraction of the mean free time between collisions at lower pressures. Each simulation ran 100 thousand time steps. We calculated the force by multiplying the shear pressure output by the area of the surfaces. Figure 10 shows the results of this calculation.

Figure 10. Thermal Creep Force (Simulation)

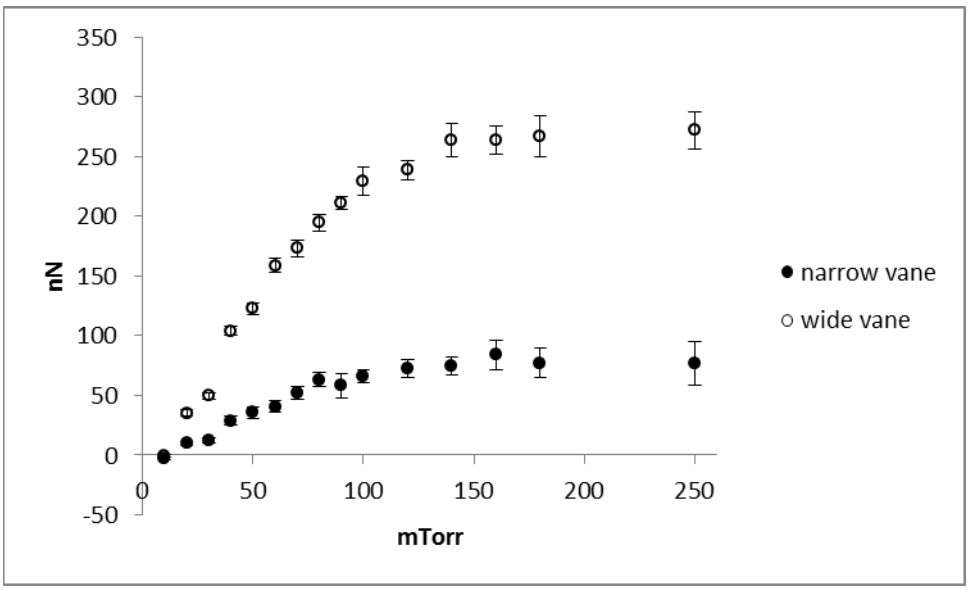

The narrow vane is 8 mm by 16 mm and the wide vane is 16 mm by 16 mm. The temperature difference on both vanes is 9 K. The characteristic length of the temperature gradient on the surface is 3.5 mm. The accommodation coefficient is 0.6. The range bars are the length of the standard deviation of the 10 segments of the trial at the reported pressure. Range bars that are not visible are hidden behind the identifying symbol. A positive force is directed from the hot side to the cold side. We believe the results at 10 mTorr to be spurious.

It is interesting to note that the values are negative at 10 mTorr (negative meaning pointing toward the hot side so that the radiometer would rotate with the black side leading). For the wide vane, the magnitude of the force is less than the standard deviation. For the narrow vane though, the force is -2.57 nN with a 1.63 nN standard deviation. None of the 10 time segments of the trial reported a positive force. This result is contrary to the experiment and theory, but similar results have been found by other researchers using the DSMC method to find thermal creep forces [1], [2]. To test the validity of this result we reran the simulation at 10 mTorr with the narrow vane in the larger simulation space used previously for the wide vane. The reported force was 2.31 nN in the positive direction (pointing toward the cold side). This demonstrates the result is sensitive to the size of the simulation space at 10 mTorr where there was a single mean free path between the vane and the boundary of the simulation space and the negative results in our trials are not to be trusted. We reran the simulation in the same manner at 50 mTorr where there were five mean free paths between the vane and the boundary of the simulation space. The reported force was 36.61 nN in the positive direction which compares favorably with the previously determined force of 35.55 nN in the positive direction with a 9.64 nN standard deviation. This suggests the results are stable with respect to the size of the simulation space when there are multiple mean free paths between the vane and the boundary of the simulation space. The trials reported here at 20 mTorr and above include more than one mean free path between the vane and the boundary of the simulation space.

We also ran trials at selected pressures with a higher accommodation coefficient. A higher accommodation coefficient resulted in larger force values as expected. Figure 11 shows these results.

Figure 11. Thermal Creep Force with Varied Accommodation (Simulation)

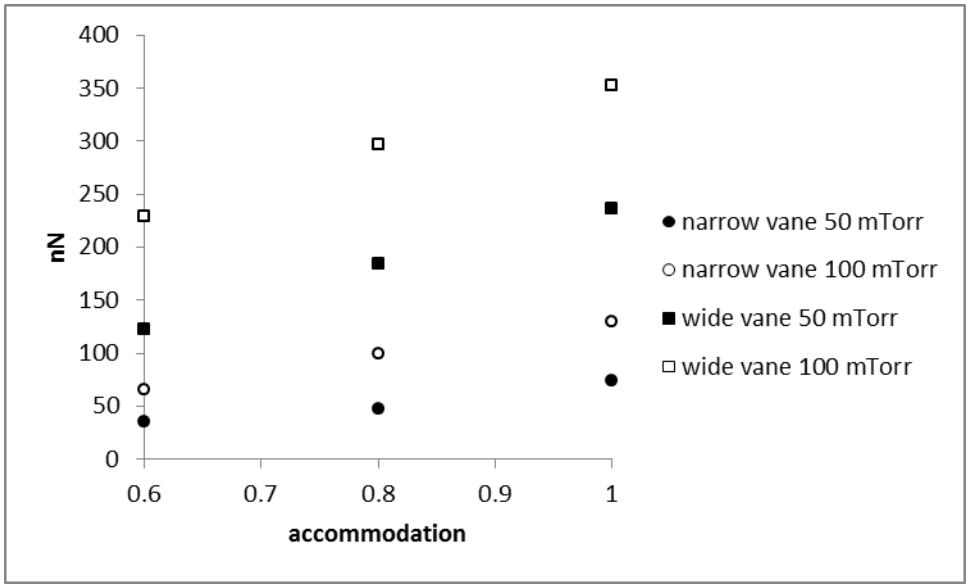

The narrow vanes are 8 mm by 16 mm and the wide vanes are 16 mm by 16 mm. The temperature difference on both vanes is 9 K. The characteristic length of the temperature gradient on the surface is 3.5 mm.

B. DRAG FORCE SIMULATIONS

We ran drag force simulations identical to the thermal creep simulations with two exceptions. First, we modeled the vanes as a single rectangular object with a temperature of 293 K. Second, collisions between the vane and particles were calculated as if the vane were rotating at 10 radians per second around an axis 4 mm from the edge of the vane though the vane was not actually rotating in the simulation space. Figures 12 and 13 show the results of these trials.

Figure 12. Drag Force at 10 rad/s (Simulation)

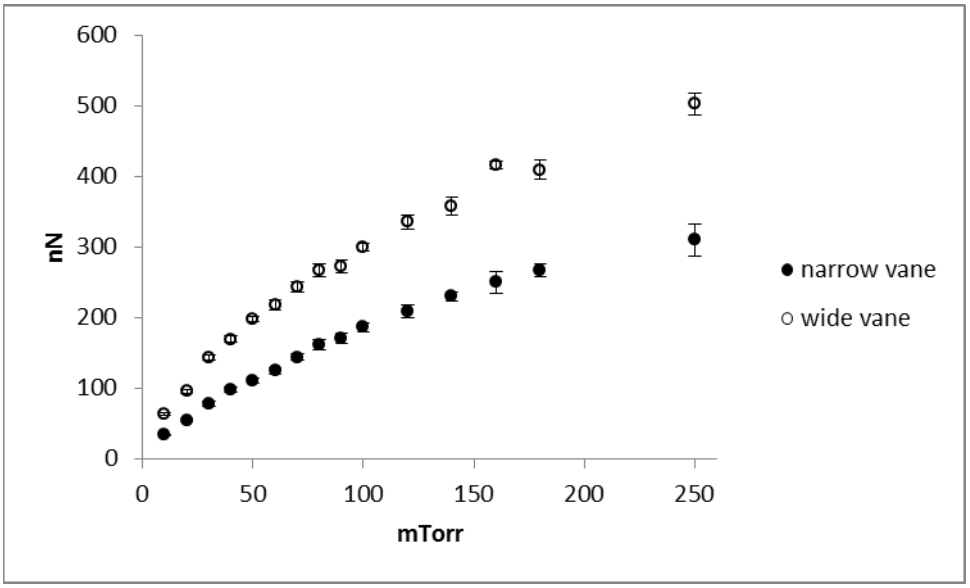

The narrow vane is 8 mm by 16 mm and the wide vane is 16 mm by 16 mm. Particle-surface collisions are calculated as if the vane is rotating about a point 4 mm beyond its edge. The accommodation coefficient is 0.6.

Figure 13. Drag Force with Varied Accommodation (Simulation)

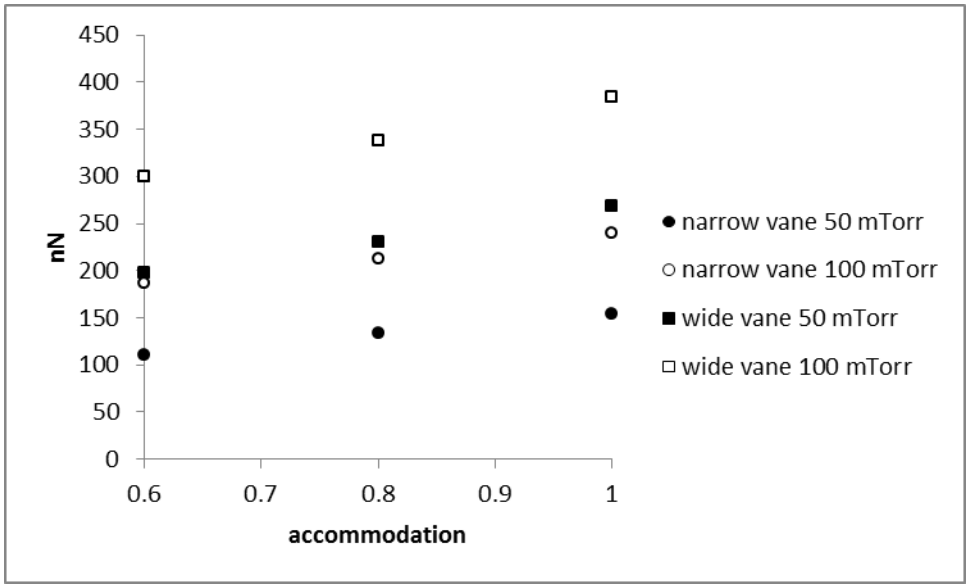

The narrow vane is 8 mm by 16 mm and the wide vane is 16 mm by 16 mm. Particle-surface collisions are calculated as if the vane is rotating at 10 rad/s about a point 4 mm beyond its edge.

Additionally, we ran a number of drag force simulations with the segmented vanes used in the thermal creep simulations to observe the effect of the segmentation. As seen in Figure 14, the segmentation does not appreciably change the drag force results leading us to assume the segmentation did not appreciably change the thermal creep force results either.

Figure 14. Drag Force with Segmented and Unsegmented Vanes (Simulation)

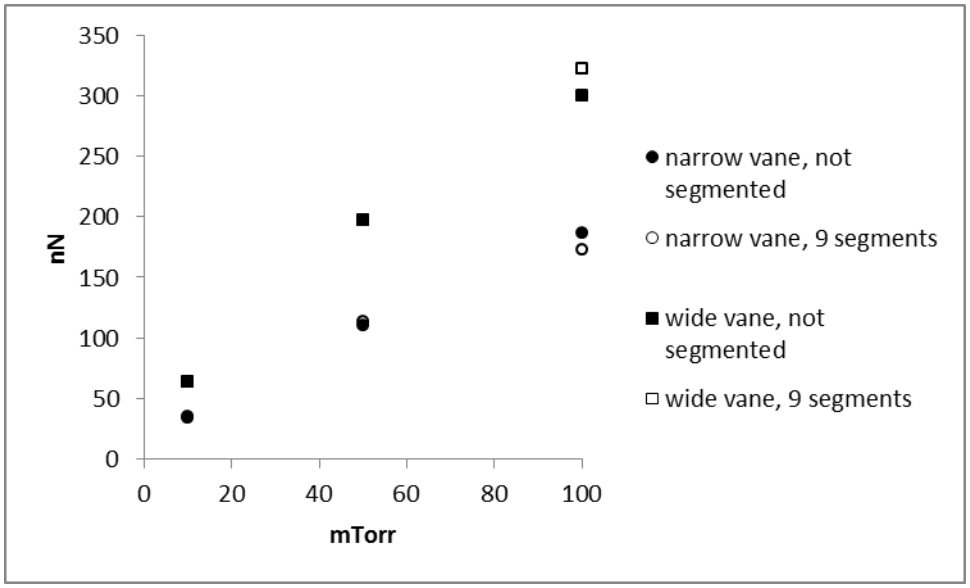

The effect of segmentation is negligible at 10 and 50 mTorr. In our simulation setup, statistical fluctuations are greater at higher pressures explaining the slight differences at 100 mTorr.

C. ANGULAR SPEED

We calculated the angular speed predicted by the simulations in the same manner as we calculated the angular speed predicted by theory,

$$\omega = \omega_0 \frac{r_{tc} F_{TC}}{r_d F_D}, \tag{4.1}$$

where ω_0 is the angular speed in the simulation. This method is possible because the drag force is linearly proportional to velocity at these pressures as seen in equation (3.22) and both forces scale linearly with the number of vanes on the radiometer. Figures 15 and 16 report the angular speed predicted by the simulations. We omitted the results at 10 mTorr because of the questionable nature of the results of our thermal creep simulations at that pressure.

Figure 15. Angular Speed (Simulation)

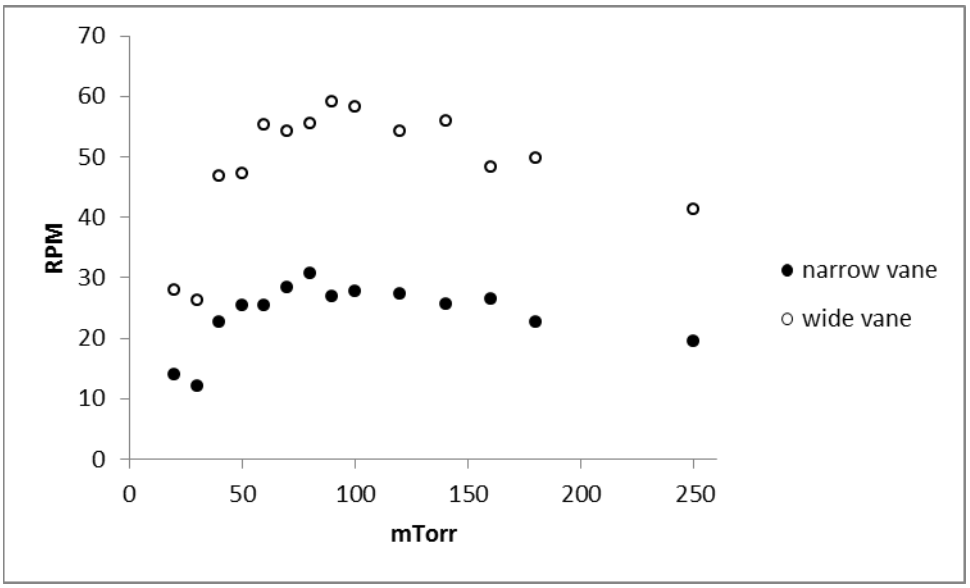

The narrow vane is 8mm by 16mm and the wide vane is 16 mm by 16 mm. Both vanes have a 4 mm stem connecting them to the spindle axis. The temperature difference on both vanes is 9 K. The characteristic length of the temperature gradient on the surface is 3.5 mm. The accommodation coefficient is 0.6. Positive angular speed represents rotation with the cold side leading.

Figure 16. Angular Speed with Varied Accommodation (Simulation)

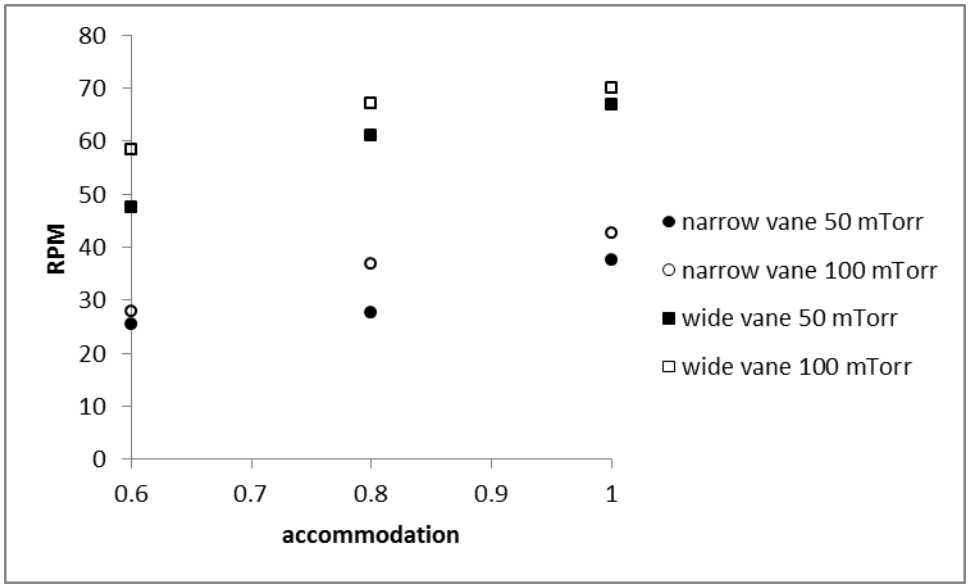

The narrow vane is 8 mm by 16 mm and the wide vane is 16 mm by 16 mm. Both vanes have a 4 mm stem connecting them to the spindle axis. The temperature difference on both vanes is 9 K. The characteristic length of the temperature gradient on the surface is 3.5 mm. Positive angular speed represents rotation with the cold side leading.

V. COMPARISON OF EXPERIMENT, THEORY, AND SIMULATIONS

In both the simulations and theory of the thermal creep force, the force rises as a function of pressure at very low pressures then becomes almost constant as a function of pressure at relatively higher pressures. Quantitatively, the differences at most pressures are less than an order of magnitude. A qualitative difference does stand out, though. The simulations show the force on the narrow vane and the wide vane asymptotically approaching different values as the pressure increases while the theory has the force on the vanes asymptotically approaching similar values. Figure 17 compares the simulation results and theory predictions at the range of pressures examined. We omitted the simulation data points at 10 mTorr because of the questionable validity of our simulation parameters at that pressure.

Figure 17. Thermal Creep Force (Simulation and Theory)

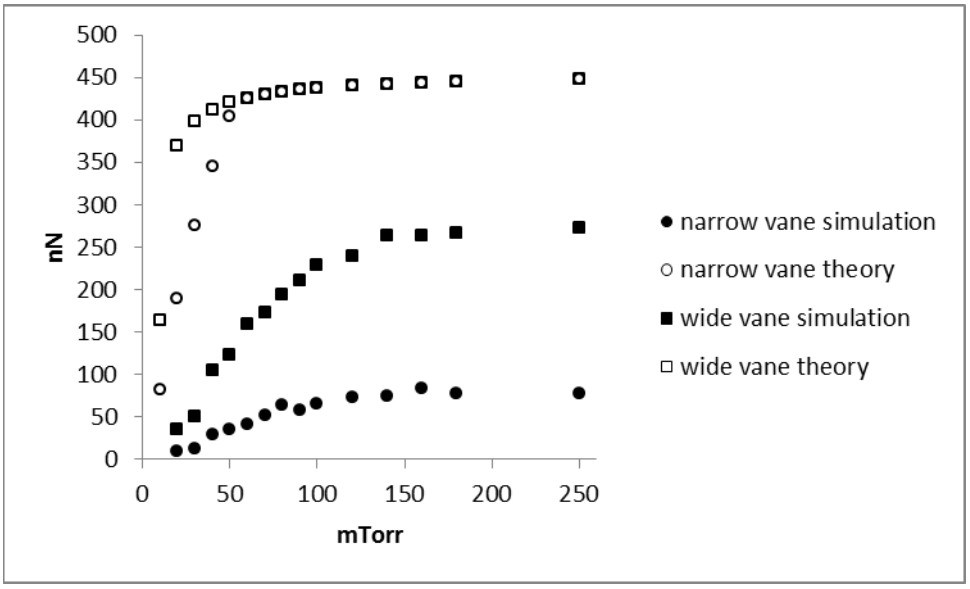

The narrow vanes are 8 mm by 16 mm and the wide vanes are 16 mm by 16 mm. The temperature difference on the vanes is 9 K. The characteristic length of the temperature gradient on the surface is 3.5 mm. The accommodation coefficient is 0.6. Positive force is directed from the hot side to the cold side.

In both the simulations and the theory of the drag force, the force rises with pressure but the rate of increase decreases with pressure. The change in the rate of increase is more pronounced in the theory than the simulations. Quantitatively the agreement is very good around 100 mTorr and the differences are less than a factor of two at all pressures examined. Figure 18 compares the simulation results and theory predictions at the range of pressures examined.

Figure 18. Drag Force (Simulation and Theory)

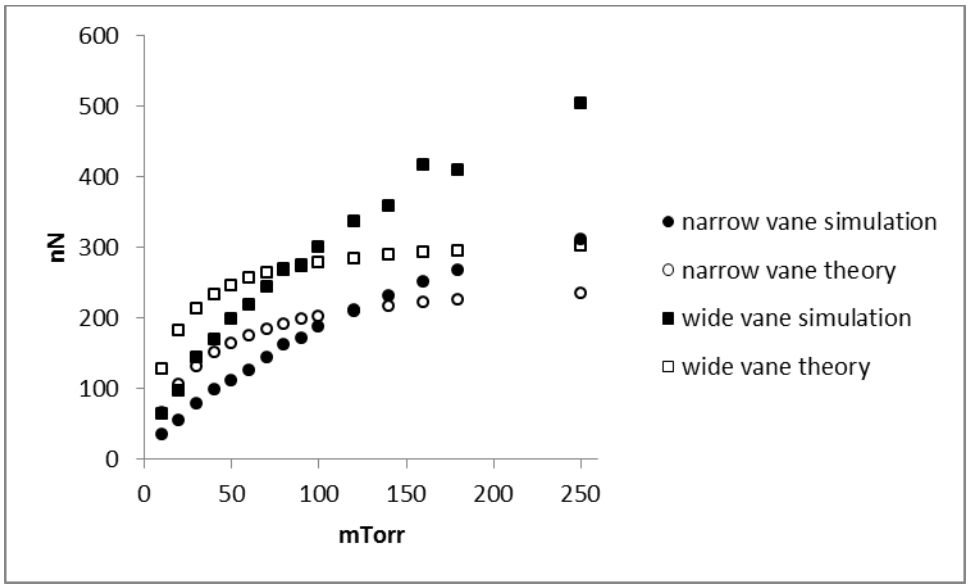

The narrow vanes are 8 mm by 16 mm and the wide vanes are 16 mm by 16 mm. The vanes have a 4 mm stem connecting them to the spindle axis. They are rotating at 10 rad/s. The accommodation coefficient is 0.6.

The experimental results, simulation predictions, and theory predictions of the angular speed of both radiometers have a peak as a function of pressure between 20 mTorr and 90 mTorr. Quantitatively the differences at most pressures are less than an order of magnitude. The theory is better than the simulations at predicting the experimental results for the narrow vane and the opposite is true for the wide vane. The decrease in the angular speed at relatively higher pressures is more pronounced in the experiment than in the simulation or theory predictions. The difference between the asymptotic force values on the narrow vane and the wide vane in the thermal creep simulations causes the simulation prediction of the angular speed to be greater for the

wide vane than the narrow vane. The theory prediction has the narrow vane faster than the wide vane at most pressures. The experimental results qualitatively match the theory predictions in this regard. Figures 19 and 20 compare the experimental results and simulation and theory predictions at the range of pressures examined.

Figure 19. Narrow Vane Angular Speed (Experiment, Simulation, and Theory)

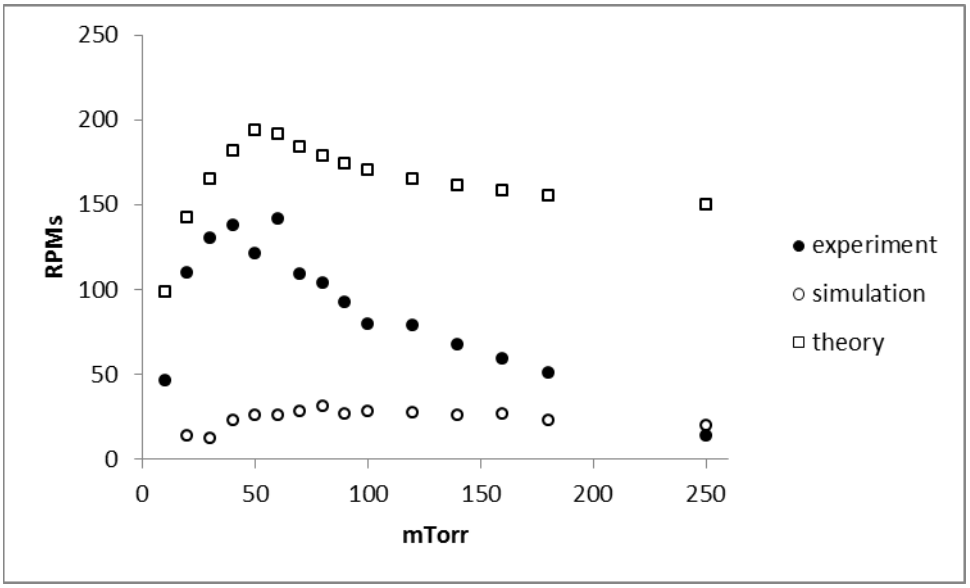

The vanes are 8 mm by 16 mm. The radiometer has 4 vanes attached to the spindle by 4 mm stems. The temperature difference on the vanes is 9 K. The characteristic length of the temperature gradient on the surfaces is 3.5 mm. Positive angular speed represents rotation with the cold side leading.

Figure 20. Wide Vane Angular Speed (Experiment, Simulation, and Theory)

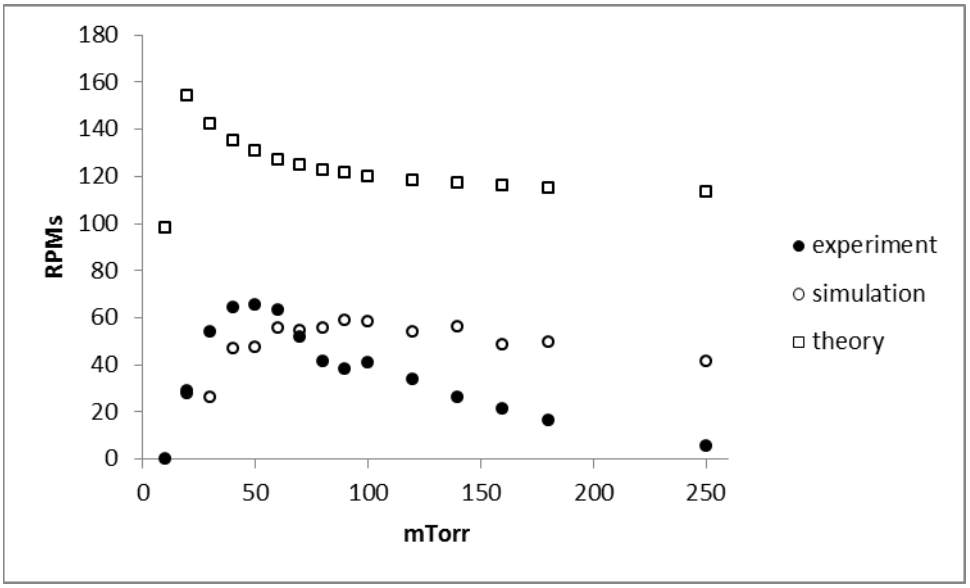

The vanes are 16 mm by 16 mm. The radiometer has 4 vanes attached to the spindle by 4 mm stems. The temperature difference on the vanes is 9 K. The characteristic length of the temperature gradient on the vanes is 3.5 mm. Positive angular speed represents rotation with the cold side leading.

The general qualitative and better than order of magnitude quantitative agreement among the results of the three methods of investigation provides confidence that each method of investigation is sound. Typically, DSMC results show better quantitative agreement with experimental results when the simulation design and parameters more closely resemble the actual conditions of the experiment, but this is often at the expense of greater computational resources. Factors which tend to cause our simulations to show a certain degree of quantitative disagreement with the experimental results include the method used to model the gradient, running separate thermal creep and drag force simulations, running simulations on static vanes thereby negating drafting and other aerodynamic effects, and simulating only the immediate volume of air surrounding the vane rather than the entire chamber. Eliminating these factors would have made the simulations time and cost excessive if not unfeasible. In our theoretical results, we chose to use reasonable assumptions for the numerical factors α, β, and x, but these values could be adjusted to better fit the experimental and simulation data. For example, Figure 21

shows the agreement between the narrow vane results if a value of 0.33 is assumed for β and x.

Figure 21. Narrow Vane Angular Speed ($\beta = x = 0.33$)

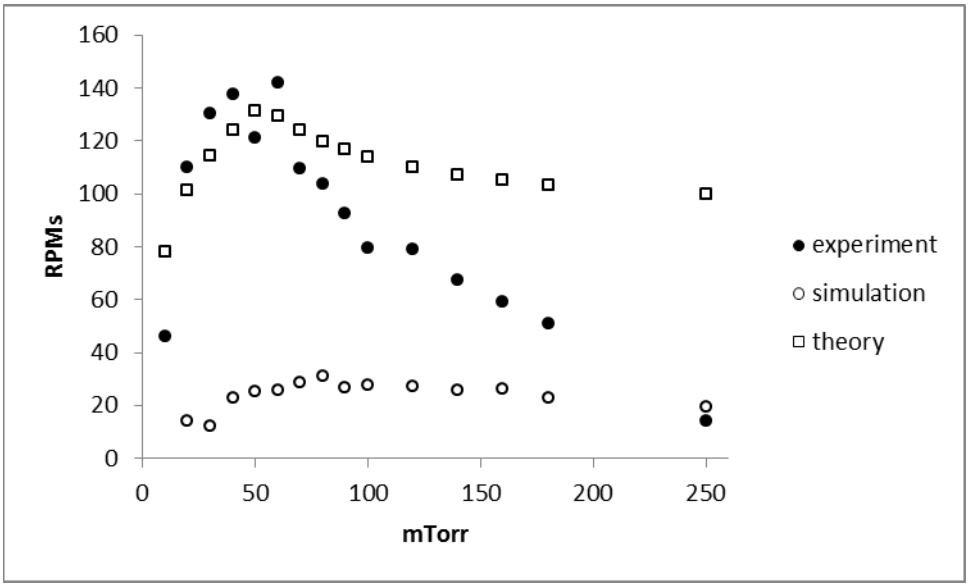

The vanes are 8 mm by 16 mm. The radiometer has 4 vanes attached to the spindle by 4 mm stems. The temperature difference on the vanes is 9 K. The characteristic length of the temperature gradient on the surfaces is 3.5 mm. Positive angular speed represents rotation with the cold side leading. The values of certain numerical factors in the theoretical results were adjusted to more closely match the experimental data.

THIS PAGE INTENTIONALLY LEFT BLANK

VI. MICRON-SCALE DEVICES AT ATMOSPHERIC PRESSURE

Microelectromechanical System (MEMS) devices can experience rarified gas effects at atmospheric pressure as their dimensions approach the mean free path of air at atmospheric pressure (68 nm). In the experiment, we observed thermal creep forces even when the width of the vane was 80 times larger than the mean free path of the surrounding air. This presents possibilities for applications of the thermal creep force on micron-scale devices at atmospheric pressure.

A. SCALING

As seen in equation (3.13) the thermal creep force scales linearly with the temperature difference on the surface. It is therefore necessary to understand the scaling relationship between the temperature differences on a millimeter-scale vane and a micron-scale vane.

Before a light is shone on a radiometer vane, the two halves are at thermal equilibrium with the environment and each other. The apparent temperature of the environment increases when the vane is exposed to a new light source. Both halves of the vane will increase in temperature until they are again at equilibrium with the environment and each other, but the black side of the vane will initially increase in temperature more quickly. As a function of time, then, the temperature difference between the two halves of the vane will start at zero before being exposed to a new light source, will increase to a maximum as the black side heats up more quickly, will decrease as the white side catches up to the black side, and will then again be zero as both halves are again in equilibrium with the environment.

The temperature difference on a vane ΔT is a function of the thermal energy of the two halves where T_H is the temperature of the hot side, T_C is the temperature of the cold side, C is the heat capacity assumed to be the same on both halves, E_H is the thermal energy of the hot side, and E_C is the thermal energy of the cold side.

$$\Delta T = T_H - T_C = \frac{1}{C}\left(E_H - E_C\right) \tag{6.1}$$

The temperature difference is a maximum when the time rates of change of the thermal energies of the two halves are equal.

$$\frac{\partial(\Delta T)}{\partial t} = 0 \rightarrow \frac{\partial E_H}{\partial t} = \frac{\partial E_C}{\partial t} \tag{6.2}$$

The temperature difference on the vanes in the experiment was not observed to vary with pressure suggesting convective heat transfer between the two sides is negligible. The time rates of change of the thermal energies are thus functions of their respective net black body radiation and the thermal conduction rate between them where σ_{SB} is the Stephan-Boltzmann constant, ε is the emissivity, A_{exp} is the surface area of one half exposed to the new light source, T_{env} is the apparent temperature of the environment, k_t is the thermal conductivity between the two halves, A_{con} is the area in contact between the two halves of the vane, and W_G is the width of the temperature gradient in the vane.

$$\frac{\partial E_H}{\partial t} = \sigma_{SB}\varepsilon_H A_{\exp}\left(T_{env}^4 - T_H^4\right) - k_t A_{con}\frac{\Delta T}{W_G} \tag{6.3}$$

$$\frac{\partial E_C}{\partial t} = \sigma_{SB}\varepsilon_C A_{\exp}\left(T_{env}^4 - T_C^4\right) + k_t A_{con}\frac{\Delta T}{W_G} \tag{6.4}$$

The temperature of the hot side of the vane can be rewritten as a function of the temperature of the cold side and the temperature difference.

$$T_H = T_C + \Delta T = T_C\left(1 + \frac{\Delta T}{T_C}\right) \tag{6.5}$$

For the vanes in the experiment and most applications, the temperature difference is much smaller than the temperature of the cold side of the vane allowing the following approximation to be made.

$$T_H^4 = T_C^4\left(1 + \frac{\Delta T}{T_C}\right)^4 \approx T_C^4 + 4T_C^3\Delta T \tag{6.6}$$

Substituting approximation (6.6) into equation (6.3) then setting equal to equation (6.4) and solving for the temperature difference provides the following result.

$$\Delta T_{\max} \approx \frac{\sigma_{SB}\left(\varepsilon_H - \varepsilon_C\right)A_{\exp}\left(T_{env}^4 - T_C^4\right)}{4\sigma_{SB}\varepsilon_H A_{\exp}T_C^3 + \frac{2k_t A_{con}}{W_G}} \tag{6.7}$$

The scaling behavior of this relation depends on whether the blackbody term, $4\sigma_{SB}\varepsilon_H A_{\exp}T_C^3$, or the thermal conductivity term, $2k_t A_{con}/W_G$, dominates the denominator. For the vanes in the experiment, the blackbody term is more than 10 times greater than the thermal conductivity term due to their relatively large areas exposed and characteristic lengths of their temperature gradients and relatively small thermal conductivity and areas of contact between the two halves.

$$\text{mm-scale, low } k_t \text{ vanes: } \Delta T_{\max} \approx \frac{\left(\varepsilon_H - \varepsilon_C\right)\left(T_{env}^4 - T_C^4\right)}{4\varepsilon_H T_C^3} \tag{6.8}$$

This expression also confirms that the magnitude of the temperature difference was not a function of the width of the vanes in the experiment.

The blackbody term is a function of two factors of physical size (A_{exp} or length times width) while the thermal conductivity term is a function of one factor of physical size and an aspect ratio (A_{con}/W_G or length times thickness divided by width). For micron-scale vanes then the thermal conductivity term is likely to dominate the denominator. The smaller dimensions will also result in the characteristic length of the temperature gradient being equal to the width of the vane. Assuming the top and bottom of the vane are both exposed to the light source, the following is an approximate expression for the maximum temperature difference on a MEMS vane where W is the width of the vane and H is the height or thickness of the vane.

$$\text{MEMS vanes: } \Delta T_{\max} \approx \frac{\sigma_{SB}\left(\varepsilon_H - \varepsilon_C\right)W^2\left(T_{env}^4 - T_C^4\right)}{2k_t H} \tag{6.9}$$

or

$$\Delta T_{\max} \propto \frac{W^2}{H} \tag{6.10}$$

or

$$\frac{\Delta T_{\max}}{W} \propto \frac{W}{H} \tag{6.11}$$

The temperature gradient is thus a function of the aspect ratio of the width (which affects the net blackbody radiation) to the thickness (which affects the thermal

conductivity). It is not a function of the length (which affects both). The temperature difference is simply the roughly constant temperature gradient times the width.

Ignoring slip length and edge corrections for the purpose of developing a scaling relation, the thermal creep force from equation (3.13) is linearly proportional to the length and temperature difference of the vane.

$$F_{TC} \propto \Delta T L \tag{6.12}$$

Combining this result with equation (6.10) provides the following scaling relationship for the thermal creep force on a MEMS vane.

$$F_{TC} \propto \frac{W^2 L}{H} \tag{6.13}$$

These scaling relationships are useful in two ways. Firstly, they allow results from centimeter-scale experiments to be extended into the MEMS realm. Secondly, they indicate the effect of varying the aspect ratio of a device. For a systematic use of the scaling relations, consider shrinking the horizontal vanes, while maintaining geometrical similarity (constant aspect ratios between the physical dimensions of the vanes) and increasing the pressure to its atmospheric value while maintaining a constant ratio between the physical dimensions of the vanes and the mean free path. For the scaling relations to be meaningful, the important parameters to determine experimentally are the temperature difference across the vane, the characteristic length of the temperature gradient on the vane, and the value at which thermal creep was observed. From the pressure reading, the physical dimensions of the vanes can be defined as functions of the mean free path. Then, equation (3.13) can be used to calculate the force at the pressure where the width of the vane equals the characteristic length of the temperature gradient on the surface. Scaling relationships (6.10) and (6.13) can then be used to extend the result of that calculation to estimate the temperature difference and force on a MEMS device at atmospheric pressure. Finally, the aspect ratios in the device can be modified to achieve a desired force.

To illustrate this process, consider the narrow vanes in the experiment. We observed a 9 K temperature difference, the temperature gradient had a characteristic length of 3.5 mm, and thermal creep was observed at pressures around 225 mTorr. Thus,

the width of the vane at this pressure is 35 mean free paths and the length is 70 mean free paths. The width of the vane equals the characteristic length of the temperature gradient when the vane is 3.5 mm by 7 mm and the mean free path is 0.1 mm. Using these values in equation (3.13) provides a force of 173 nN. Scaling relationships (6.10) and (6.13) then predict a 6 mK temperature difference and a 0.08 pN force on a 2.4 μm by 4.8 μm device at atmospheric pressure. If we instead wanted a force of 1 pN, relation (6.13) shows we could increase the length to 60 μm or increase the width to 8.5 μm.

Ignoring the slip length correction to the dynamic viscosity for the purpose of developing a drag force scaling relation and assuming a fixed aspect ratio, the drag force on a rotating vane from equation (3.22) is proportional to a measure of length squared.

$$F_D \propto L^2 \tag{6.14}$$

Since both the thermal creep and drag forces scale as a measure of length squared, devices of different sizes should be able to achieve comparable angular velocities at their peak pressures though the peak pressure will scale with the size of the device.

Substituting the angular velocity $U = \omega L$ and Maxwell's estimate of the dynamic viscosity $\mu = \rho C \lambda / 3$ into the Reynolds number $\mathrm{Re} = \rho U W / \mu$ provides the following scaling relation for the Reynold's number for horizontal vane radiometers operating at the same angular speed in the same gas at the same temperature,

$$\mathrm{Re} \propto \frac{LW}{\lambda}, \tag{6.15}$$

confirming a MEMS horizontal vane radiometer will remain in the Stokes' drag regime at much higher pressure than a millimeter scale device.

B. DESIGN

Thermal creep forces will occur in MEMS devices whenever a temperature gradient in the surrounding gas is parallel to a surface. A geometrically symmetrical component that is hotter than the ambient temperature will create temperature gradients in the surrounding gas and experience thermal creep forces, but they will tend to cancel due to the symmetry. Thermal creep forces that are likely to degrade device performance are created by unevenly heated components or hot components with an asymmetrical

geometry and should be considered in the design process. If properly designed, MEMS devices could even utilize thermal creep forces for energy harvesting and for sensing. Passian *et al.* designed a MEMS cantilever with pores that experiences thermal transpiration forces when exposed to a modulated laser [25]. When the modulation frequency is on the order of 1 kHz or greater the cantilever does not reach a uniform temperature creating a temperature gradient in the structure. Here we consider two designs based on our horizontal vane radiometer which establishes a temperature gradient by having two halves of differing emissivity.

The thermal conductivity of silicon is 2,600 times greater than the thermal conductivity of the paper that was used in the horizontal vane radiometer experiments. As seen in equation (6.9) the temperature difference created on a MEMS vane is inversely proportional to the thermal conductivity making low thermal conductivity polymers and ceramics better design choices than silicon or metals. Two common polymers used in MEMS fabrication are the polyimide Kapton and the epoxide SU-8. Analysis of the temperature difference on a radiometer vane made of two materials is complicated by the differing heat capacity and thermal conductivity on the two sides of the vane, but the values for Kapton and SU-8 are close enough that the scaling analysis can be used for rough estimation. The thermal conductivities of Kapton and SU-8 are 2.4 and 4 times larger than the thermal conductivity of paper respectively [26], [27], but gaps in the contact area between the two materials because of manufacturing tolerances will decrease the thermal transfer between the two sides of the vane. Tabulated emissivity values differ between sources and are difficult to find for certain materials. Emissivity values for white paper range from 0.68 to 0.93. Values for carbon, which provides the coloring in Laserjet ink, range from 0.80 to 0.95 [28]. The emissivity of Kapton is 0.57 and the emissivity of SU-8 is 0.95 [29], [30]. These values suggest the emissivity difference between Kapton and SU-8 would be even greater than the difference between white paper and black LaserJet ink. These material properties suggest that a MEMS horizontal vane radiometer made of polyimide and SU-8 could rotate with an angular velocity of the same order of magnitude as the radiometers in our experiment.

We designed a MEMS horizontal vane radiometer, as shown in Figure 22.

Figure 22. MEMS Horizontal Vane Radiometer Cross Section and Vane Structure Overhead View

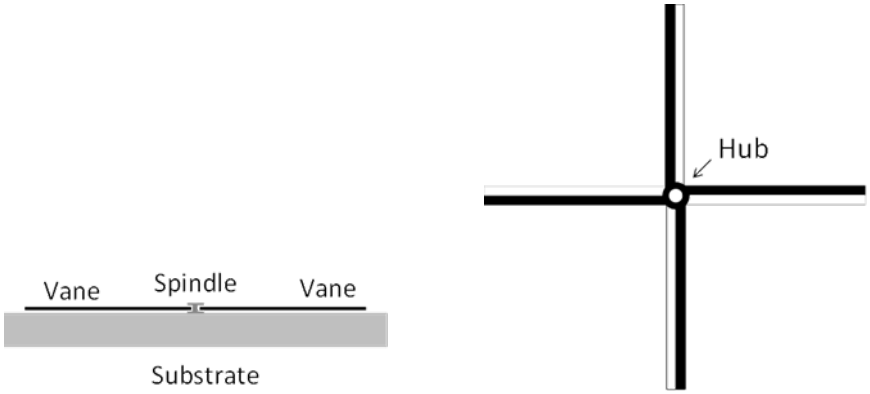

The figure on left is a cross section of a MEMS horizontal vane radiometer. The figure on the right is an overhead view of the vane structure.

The vane structure consists of a piece of Kapton and a separate piece of SU-8. Each piece consists of a circular hub and four vanes. Each piece was given its own hub to make the structure more robust. The spindle has a base and a top both of which are wider than the openings in the hubs while the spindle itself is narrower than the hub openings. This design prevents the vane structure from riding on the substrate or separating from the spindle. We used MEMS Pro L-Edit to plan the steps necessary to realize the design. The fabrication process requires 11 steps. Figures 23, 24, and 25 show a selection of the fabrication steps.

Figure 23. MEMS Horizontal Vane Radiometer Fabrication Step 5

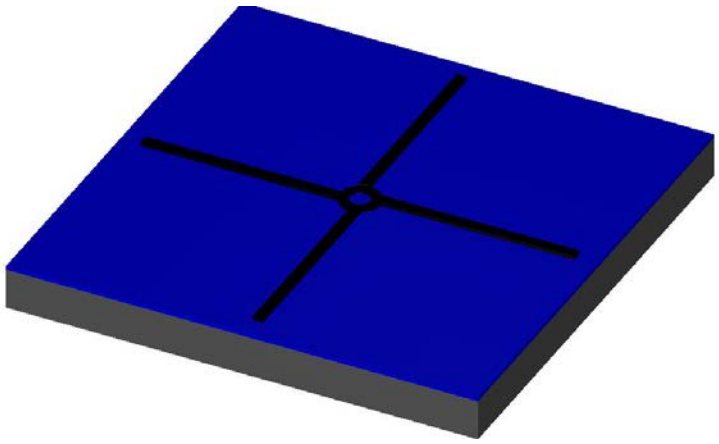

The black structure is the SU-8 portion of the radiometer. The blue is a sacrificial layer of silicon dioxide. The base of the spindle is below the sacrificial layer. The next step is to deposit a layer of Kapton.

Figure 24. MEMS Horizontal Vane Radiometer Fabrication Step 7

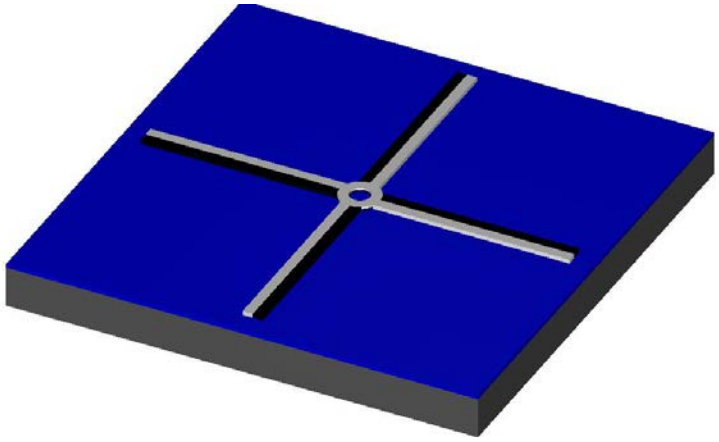

The white is the Kapton portion and the black is the SU-8 portion of the radiometer. The blue is a sacrificial later of silicon dioxide. The base of the spindle is below the sacrificial layer. The next step is to deposit another sacrificial layer.

Figure 25. MEMS Horizontal Vane Radiometer

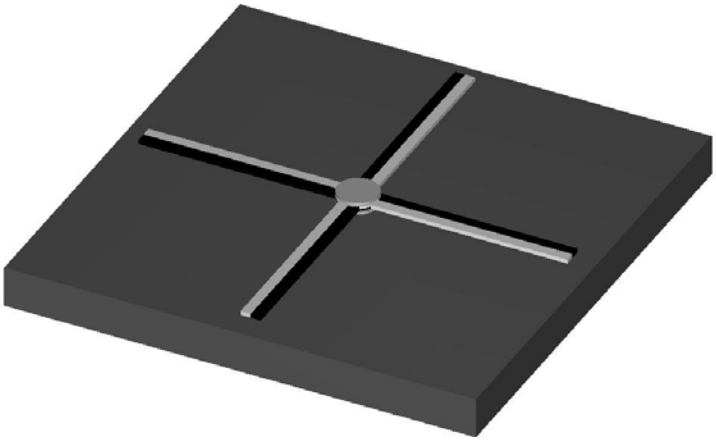

The white is the Kapton portion and the black is the SU-8 portion of the radiometer. The light grey circle is the spindle top. The vane structure is resting on the spindle base rather than the substrate. A narrow spindle runs through the hub.

C. APPLICATIONS

There are numerous potential applications of the thermal creep force on MEMS devices. One of the most interesting is energy harvesting. Consider an electric generator with a horizontal vane radiometer rotor (see Figure 26).

Figure 26. Simplified Electric Generator with Horizontal Vane Radiometer Rotor

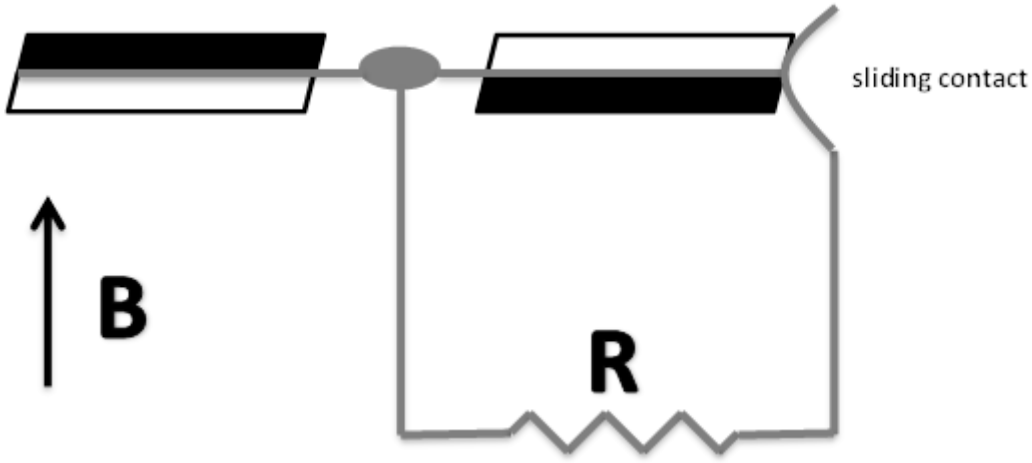

The vanes have a conductive wire along their axis. Rotation in the magnetic field creates an electromotive force in the wire. The circuit closes when the vane sweeps the sliding contact. This is a simplified diagram of a DC generator to facilitate calculation of the voltage produced. A real rotor could be seated inside a cylinder with the vanes in contact with the casing so the circuit is always closed.

The voltage produced is proportional to the angular velocity, magnetic field *B*, and the length of the vanes squared found by integrating the magnetic force, $\vec{v} \times \vec{B}$, over the length of a vane.

$$V = \frac{\omega B L^2}{2} \tag{6.16}$$

A radiometer with 100 μm vanes operating a 10 rad/s in a 1 T magnetic field would generate 50 nV. The small size though would allow numerous such devices to fit on a single chip. 1,000 connected in series would generate 50 μV.

Alternatively, consider a bicolored cantilever beam with a thin piezoelectric film at its base (see Figure 27).

Figure 27. Cantilever Beam with Piezoelectric Base

The piezoelectric film is in grey at the base of the cantilever beam. The deflection of the beam will create a tensile stress in piezoelectric film along its length which will generate a potential difference orthogonal to the stress.

The voltage produced in the piezoelectric film is as follows where d_{31} is the appropriate piezoelectric coefficient, F is the total force assumed to be applied at the free end of the cantilever beam, L is the length of the cantilever beam, W is the width of the cantilever bean, t is the thickness of the piezoelectric film, ε is the permittivity of the piezoelectric film, and I is the area moment of inertia of a cross section of the cantilever beam [31].

$$V = \frac{d_{31} FLWt}{2\varepsilon I} \tag{6.17}$$

Substituting $W^3H/12$ for the area moment of inertia where H is the height or thickness of the cantilever beam and multiplying by 3/8 to account for the fact the thermal creep force will be uniformly distributed over the cantilever beam and not applied solely at the free end provides the following result.

$$V = \frac{9 d_{31} FLt}{4\varepsilon W^2 H} \tag{6.18}$$

Combining equations (6.13) and (6.18) provides the following as the dependence of the voltage on the dimensions of the cantilever beam.

$$V \propto \frac{L^2}{H^2} \tag{6.19}$$

The voltage is thus a function of the ratio of the length to the thickness of the cantilever beam rather than the overall size and completely independent of the width of the cantilever beam. The devices can therefore be as small as MEMS manufacturing technology will allow and connected in series to create a higher overall voltage. According to equation (6.18), a 100 μm by 10 μm by 1μm cantilever beam able to produce 1 pN of thermal creep force with a 1 μm thick zinc oxide film at is base would produce 150 nV. 1,000 such devices connected on a single chip would produce 150 μV. The disadvantage of this design compared to the rotor design is the need for a periodic interrupter of the light to maintain a continuous alternating current.

THIS PAGE INTENTIONALLY LEFT BLANK

VII. CONCLUSION

We have investigated the thermal creep shear force through experiment, kinetic theory calculations, and the DSMC simulations. All three investigations show the force acting from the hot to the cold side of the surface. The theory and the simulations both show the force rising with pressure and asymptotically approaching a constant value though the theory shows the force on both vanes approaching the same value while the simulations show the force on the two vanes approaching different values. The theory and the simulations both show the decrease in the radiometer's angular speed as a function of pressure at relatively higher pressures to be the result of increasing drag force rather than decreasing thermal creep force.

Left unexplained by our investigation is why the theory is better at predicting the experimental results for the narrow vane and the simulation results are better at predicting the experimental results for the wide vane. This suggests that at least two of the three methods of investigation, while good, can be further improved upon. There are potential areas of future work which would provide additional insight in all three methods of investigation. In our experiment, we measured angular speed which is the result of all forces on the moving radiometer. Additional insight on the thermal creep force in particular could be achieved by static force measurements on a fixed vane. In our theory, we made a quasi-static assumption and made assumptions about the temperature distribution of the gas. Adding dynamic effects to the theory and experimentally or in simulation directly observing the temperature distribution in the gas and incorporating the results could improve our theory. In our simulations, the thermal creep force and drag force were determined in separate trials. Trials with both a rotating vane and a temperature gradient could reveal any second order effects from the interaction of drag and thermal creep.

We also provided scaling relations between millimeter scale and MEMS horizontal vane radiometers, a design for a MEMS horizontal vane radiometer, and two potential applications of the thermal creep force for energy harvesting with MEMS

devices. Future work to optimize these applications would improve the modest voltage output we predicted and possibly create useful devices.

APPENDIX A. EINSTEIN EFFECT

In Einstein's development of his effect, he simplified the behavior of the gas by assuming all gas molecules moved in only one axis direction at a time. In a cubic volume, 1/6 of the molecules leave the volume through any one face of the cube. The number of molecules impacting a surface of area A from one direction per unit time is then

$$\frac{1}{6}nAv \tag{7.1}$$

where n is the number density and v is the average speed of a gas molecule. The difference in momentum between molecules of mass m coming from the hot side and the cold side of a surface perpendicular to a temperature gradient is

$$mv_+ - mv_- \tag{7.2}$$

where v_+ and v_- are the speeds of molecules from the hot and cold sides respectively. In a gas with no net mass flow, the number of molecules impacting the surface per unit time from each direction is equal. The force on the surface is then the number of molecules impacting from one direction per unit time times the difference in momentum between molecules coming from opposing sides.

$$F_{Einstein} = -\frac{1}{6}nAmv\left(v_+ - v_-\right) \tag{7.3}$$

where the temperature gradient is in the positive direction. Rewriting v as the average of v_+ and v_-, we have

$$F_{Einstein} = -\frac{1}{6}nAm\left(\frac{v_+ + v_-}{2}\right)\left(v_+ - v_-\right) = -\frac{1}{12}nAm\left(v_+^2 - v_-^2\right) \tag{7.4}$$

Substituting $3k_BT/2 = mv^2/2$ we have

$$F_{Einstein} = -\frac{1}{4}nk_B\left(T_+ - T_-\right)A. \tag{7.5}$$

Assuming the temperature of molecules arriving from the hot and the cold sides were each established one mean free path away,

$$T_+ = T + \lambda\frac{dT}{dx} \tag{7.6}$$

and

$$T_{-} = T - \lambda \frac{dT}{dx} \tag{7.7}$$

where dT/dx is the temperature gradient. Substituting equations (7.6) and (7.7) into equation (7.5) we have

$$F_{Einstein} = -\frac{1}{2} n k_B \lambda \frac{dT}{dx} A. \tag{7.8}$$

Then substituting the ideal gas equation where P is pressure we have

$$F_{Einstein} = -\frac{1}{2} \frac{P\lambda}{T} \frac{dT}{dx} A. \tag{7.9}$$

Finally, assuming that the temperature gradient is proportional to the temperature difference between the hot and the cold sides of the vane ΔT divided by the mean free path, the area is a mean free path wide strip the length of the perimeter L_p, and dropping the numerical factor as this is a qualitative, order of magnitude expression, we have [11]

$$F_{Einstein} = -P\lambda \frac{\Delta T}{T} L_p. \tag{7.10}$$

In terms of kinetic theory quantities,

$$F_{Einstein} \propto -\frac{\Delta T L_p}{\sigma_{CS}}. \tag{7.11}$$

Scandurra *et al.* find a similar relationship using the Chapman-Enskog method but include a factor of $2-\alpha$ to include recoil effects when the molecules are not fully accommodated by the surface. [4]

It is also possible to relate the force to the heat flow through an open area of the same size and orientation to the temperature gradient. The difference in energy between molecules coming from the hot side and the cold side is

$$\frac{1}{2} m v_{+}^2 - \frac{1}{2} m v_{-}^2. \tag{7.12}$$

The heat flow is then the number of molecules passing through from one direction per unit time times the energy difference between molecules coming from opposite directions or

$$\phi A = -\frac{1}{6} n A v \left(\frac{1}{2} m v_{+}^2 - \frac{1}{2} m v_{-}^2 \right) = -\frac{1}{12} n A m v \left(v_{+}^2 - v_{-}^2 \right) \tag{7.13}$$

where ϕ is the heat flux. Comparing equation (7.4) to (7.13) makes clear that [11]

$$F_{Einstein} = \frac{\phi A}{\nu}. \tag{7.14}$$

THIS PAGE INTENTIONALLY LEFT BLANK

APPENDIX B. EXAMPLE THERMAL CREEP INPUT SCRIPT

```
seed            7092015
dimension       3
global          gridcut 0.001
boundary        o o o
create_box      -0.009 0.009 -0.013 0.013 -0.005 0.005
create_grid     35 50 19 block * * *
global          temp 293
global          nrho 1.65e21 fnum 9.07e6
global          gravity 9.81 0 0 -1
species         air.species N2 O2
mixture         air N2 frac .79
mixture         air O2 frac .21
read_surf       1 data.cold_vane8mm
surf_collide    1 diffuse 293 .6
surf_modify     collide 1 1
read_surf       2 data.mid_vane1
surf_collide    2 diffuse 294.125 .6
surf_modify     collide 2 2
read_surf       3 data.mid_vane2
surf_collide    3 diffuse 295.25 .6
surf_modify     collide 3 3
```

```
read_surf           4 data.mid_vane3
surf_collide        4 diffuse 296.375 .6
surf_modify         collide 4 4
read_surf           5 data.mid_vane4
surf_collide        5 diffuse 297.5 .6
surf_modify         collide 5 5
read_surf           6 data.mid_vane5
surf_collide        6 diffuse 298.625 .6
surf_modify         collide 6 6
read_surf           7 data.mid_vane6
surf_collide        7 diffuse 299.75 .6
surf_modify         collide 7 7
read_surf           8 data.mid_vane7
surf_collide        8 diffuse 300.875 .6
surf_modify         collide 8 8
read_surf           9 data.hot_vane8mm
surf_collide        9 diffuse 302 .6
surf_modify         collide 9 9
collide             vss air air.vss
collide_modify      vremax 1000 yes
create_particles    air n 0
fix                 in inflow air all
timestep            1e-7
```

compute	1 surf air shx shy shz
fix	1 ave/surf 1 100000 100000 c_1
dump	1 surf 100000 dump.vane50tcbb id v1x v1y v1z v2x v2y v2z v3x v3y v3z f_1
compute	2 surf air shx shy shz
fix	2 ave/surf 1 10000 10000 c_2
dump	2 surf 10000 dump.vane50tenthtcbb id v1x v1y v1z v2x v2y v2z v3x v3y v3z f_2
stats	1000
stats_style	step
run	100000

THIS PAGE INTENTIONALLY LEFT BLANK

APPENDIX C. EXAMPLE DRAG INPUT SCRIPT

```
seed                7092015
dimension           3
global              gridcut 0.001
boundary            o o o
create_box          -0.009 0.009 -0.013 0.013 -0.005 0.005
create_grid         35 50 19 block * * *
global              temp 293
global              nrho 1.65e21 fnum 9.07e6
global              gravity 9.81 0 0 -1
species             air.species N2 O2
mixture             air N2 frac .79
mixture             air O2 frac .21
read_surf           1 data.vane
surf_collide        1 diffuse 293 .6 rotate 0 -.012 0 0 0 10
surf_modify         collide 1 1
collide             vss air air.vss
collide_modify      vremax 1000 yes
create_particles    air n 0
fix                 in inflow air all
timestep            1e-7
compute             1 surf air shx shy shz
fix                 1 ave/surf 1 100000 100000 c_1
```

dump	1 surf 100000 dump.vane50rvbb id v1x v1y v1z v2x v2y v2z v3x v3y v3z f_1
compute	2 surf air shx shy shz
fix	2 ave/surf 1 10000 10000 c_2
dump	2 surf 10000 dump.vane50tenthrvbb id v1x v1y v1z v2x v2y v2z v3x v3y v3z f_2
stats	1000
stats_style	step
run	100000

LIST OF REFERENCES

[1] N. Selden, C. Ngalande, N. Gimelshein, S. Gimelsein and A. Ketsdever, "Origins of radiometric forces on a circular vane with a temperature gradient," *Journal of Fluid Mechanics*, vol. 634, pp. 419–431, 2009.

[2] C. White, C. Colombo, T. J. Scanlon, C. R. McInnes and J. M. Reese, "Rarefied gas effects on the aerodynamics of high area-to-mass ratio spacecraft in orbit," *Advances in Space Research*, vol. 51, pp. 2112–2124, 2013.

[3] A. Ketsdever, N. Gimelshein, S. Gimelshein and N. Selden, "Radiometric phenomena: From the 19th to the 21st century," *Vacuum*, vol. 86, pp. 1644–1662, 2012.

[4] M. Scandurra, F. Iacopetti and P. Colona, "Gas kinetic forces on thin plates in the presence of thermal gradients," *Physical Review E*, vol. 75, no. 2, pp. 0263081–0263085, 2007.

[5] W. Crookes, "Researches on the atomic weight of thallium," *Philosophical Transactions of the Royal Society of London*, vol. 163, pp. 277–330, 1873.

[6] W. Crookes, "On attraction and repulsion resulting from radiation," *Philosophical Transactions of the Royal Society of London*, vol. 164, pp. 501–527, 1874.

[7] O. Reynolds, "On the forces caused by evaporation from, and condensation at, a surface," *Proceedings of the Royal Society of London*, vol. 22, pp. 401–401, 1874.

[8] O. Reynolds, "On certain dimensional properties of matter in the gaseous state," *Philosophical Transactions of the Royal Society of London*, vol. 170, pp. 727–845, 1879.

[9] J. C. Maxwell, "On stresses in rarified gases arising from inequalities of temperature," *Philosophical Transactions of the Royal Society of London*, vol. 170, pp. 231–256, 1879.

[10] S. Song and M. M. Yovanovich, "Correlation of thermal accommodation coefficient for 'engineering' surfaces," in *National Heat Transfer Conference*, Pittsburgh, 1987.

[11] L. B. Loeb, *The Kinetic Theory of Gases*, New York, NY: McGraw-Hill Book Company, 1934.

[12] M. Czerny and G. Hettner, "Measurement of thermal slip gases," *Magazine for Physics*, vol. 30, no. 1, pp. 258–267, 1924.

[13] R. Marvin, “Radiometric forces on the Crookes radiometer,” M.S. thesis, Dept. Physics, Naval Postgraduate School, Monterey, CA, 2012.

[14] A. Lopez, J. Lopez, A. Larraza and D. Wolfe. (2015, Dec. 2). Maxwell and Crookes Radiometers. [YouTube video]. Available: https://www.youtube.com/watch?v=6jhNyA-SoSA

[15] D. Wolfe, A. Larraza and A. Garcia, “A horizontal vane radiometer: Experiment, theory, and simulation,” *Physics of Fluids*, vol. 28, no. 3, p. 037103, 2016.

[16] E. H. Kennard, *Kinetic Theory of Gases*, New York, NY: McGraw-Hill Book Company, 1938.

[17] S. Chapman and T. G. Cowling, *The Mathematical Theory of Non-Uniform Gases*, Cambridge, UK: University Press, 1952.

[18] Y. H. Kuo, “On the flow of an incompressible viscous fluid past a flat plate at moderate Reynolds numbers,” *The Journal of Mathematics and Physics*, vol. 32, pp. 83–101, 1953.

[19] A. M. Jones and J. G. Knudsen, “Drag coefficients at low Reynolds numbers for flow past immersed bodies,” *A.I.Ch.E. Journal*, vol. 7, no. 1, pp. 20–25, 1961.

[20] Z. Janour, *Resistance of a Plate in Parallel Flow at Low Reynolds Numbers*, Washington, DC: NACA TM 1316, 1951.

[21] G. Bird, *Molecular Gas Dynamics and the Direct Simulation of Gas Flows*, Oxford, UK: Clarendon Press, 1994.

[22] F. J. Alexander, A. L. Garcia and B. J. Alder, “Cell size dependence of transport coefficients in stochastic particle algorithms,” *Physics of Fluids*, vol. 10, no. 6, pp. 1540–1542, 1998.

[23] A. L. Garcia and W. Wagner, “Time step truncation error in direct simulation Monte Carlo,” *Physics of Fluids*, vol. 12, no. 10, pp. 2621–2633, 2000.

[24] M. A. Gallis, J. R. Torczynski, S. J. Plimpton, D. J. Rader and T. Koehler, “Direct simulation Monte Carlo: The quest for speed,” in *Proceedings of the 29th Rarefied Gas Dynamics Symposium*, Xi’an, CN, 2014.

[25] A. Passian, R. J. Warmack, T. L. Ferrell and T. T, “Thermal transpiration at the microscale: A Crookes cantilever,” *Physical Review Letters*, vol. 90, no. 12, p. 124503, 2003.

[26] Kapton Summary of Properties. DuPont. (n.d.). [Online]. Available: http://www.dupont.com/content/dam/dupont/products-and-services/membranes-

and-films/polyimde-films/documents/DEC-Kapton-summary-of-properties.pdf. Accessed 19 February 2016.

[27] SU-8 Table of Properties. Micro Chem. (n.d.). [Online]. Available: http://www.microchem.com/pdf/SU-8-table-of-properties.pdf. Accessed 19 February 2016.

[28] Emissivity Table. (n.d.). ThermoWorks. [Online]. Available: http://www.thermoworks.com/emissivity_table.html. Accessed 19 February 2016.

[29] Emissivity of Materials. (n.d.). Electro Optical Industries. [Online]. Available: http://www.electro-optical.com/eoi_page.asp?h=Emissivity%20of%20Materials. Accessed 19 February 2016.

[30] T. Winterstein, M. Staab, C. Nakic, H.-J. Feige, J. Vogel and H. F. Schlaak, "SU-8 electrothermal actuators: Optimization of fabrication and excitation for long-term use," *Micromachines*, vol. 5, pp. 1310–1322, 2014.

[31] C. Liu, *Foundations of MEMS*, Upper Saddle River, NJ: Pearson Prentice Hall, 2006.

THIS PAGE INTENTIONALLY LEFT BLANK

INITIAL DISTRIBUTION LIST

1. Defense Technical Information Center
   Ft. Belvoir, Virginia

2. Dudley Knox Library
   Naval Postgraduate School
   Monterey, California